Analysis of Differential Motions at the Hanford, Washington and Livingston, Louisiana LIGO Sites

Alan Rohay, Pacific Northwest National Laboratory

1.0 Introduction

Seismic measurements taken simultaneously at the Corner and two Ends of the Laser Interferometer Gravitational Wave Observatory sites are used to estimate the relative position differences between the Corner and each of the Ends. This analysis is conducted for data taken at the Livingston, Louisiana and Hanford, Washington, LIGO sites, where previous studies primarily described the motions at each measurement location independently from each other, and the analysis was conducted in the frequency range from 0.1 to 100 Hz. The analysis of the high-frequency vibrations primarily supported the design of passive vibration-isolation systems. In this study, the analysis is conducted on frequencies below 1 Hz, where active feedback systems may be used to maintain arm lengths within a prescribed tolerance.

A significant reduction of relative motion (compared to independent motions) is observed along the two perpendicular arms at the Hanford LIGO site. The reduction is greatest along the Northwest Arm, especially for the lower frequencies that comprise the largest ground motions. At Livingston, an increase in relative motion results, comparable to that which would be expected from completely un-correlated motions at the different locations. These differences are explained by the dominance of relatively fast-propagating waves at Hanford compared to slow-propagating waves at Livingston.

Cumulative histograms of differential motion along the arms of the Hanford LIGO site indicate that the 90th-percentile differential displacement has an amplitude of approximately 4×10^{-7} m in the 100-250 mHz band. This compares to an approximate 90th-percentile value at the Livingston LIGO site on the order of 4×10^{-6} m. These values correspond to strains, rotations, or tilts of the 4-km arms by 0.1 and 1.0 parts per billion for the Hanford and Livingston LIGO sites, respectively.

2.0 Data Description

Measurements were taken at the Livingston, Louisiana site from October 26 to November 2, 1995. These measurements were taken with three independently-operating seismometer and recorder systems that were timed to within 0.25 milliseconds using continuously-synchronizing GPS receivers. Earlier data collected at Hanford in 1994 were collected one location at a time, so synchronous data were collected there from January4-8, 1996 to pro-

vide the data for the current analysis. Data were sampled at 250 samples/second and 125 samples/second at Livingston and Hanford, respectively. For the purposes of this analysis of low-frequency correlation, both sets of data were decimated to a uniform 25 samples/second. A twelve-hour time series was analyzed for each of the two sites. At Livingston, the data used are from the period 1200 - 2400 GMT on Day 303 (6:00 a.m. CST to 6:00 p.m. CST on Monday, October 30, 1995). At Hanford, the data used are from the period from 0200 - 1400 GMT on Day 005 (6:00 p.m. January 4 to 6:00 a.m. January 5, 1996). The time period for the Livingston data was chosen because it represented a period when the noise amplitudes near 0.2 Hz were at the maximum observed during the recording period. (Note: data was not available from South End north component for this time period.) At Hanford, the time period avoided complications from instrument transients.

The seismometers were oriented so that the "North" axis of the horizontal component seismometer was aligned with the LIGO arm nearest the north-south direction, as shown in Figure 1. Seismometers were calibrated before and after the deployments, and system noise measurements were made that indicate the seismic noise is resolved above 0.1 Hz. The calibration results confirmed the responses measured by the manufacturer, showing that two of the instruments had an equivalent 20-second-period seismometer response and the third instrument had that of a 30-second-period seismometer. Although either response is sufficiently flat to ground velocity above 0.1 Hz, there is a slight phase response difference of the 30-second seismometer that was corrected to be the same as the two 20-second instruments.

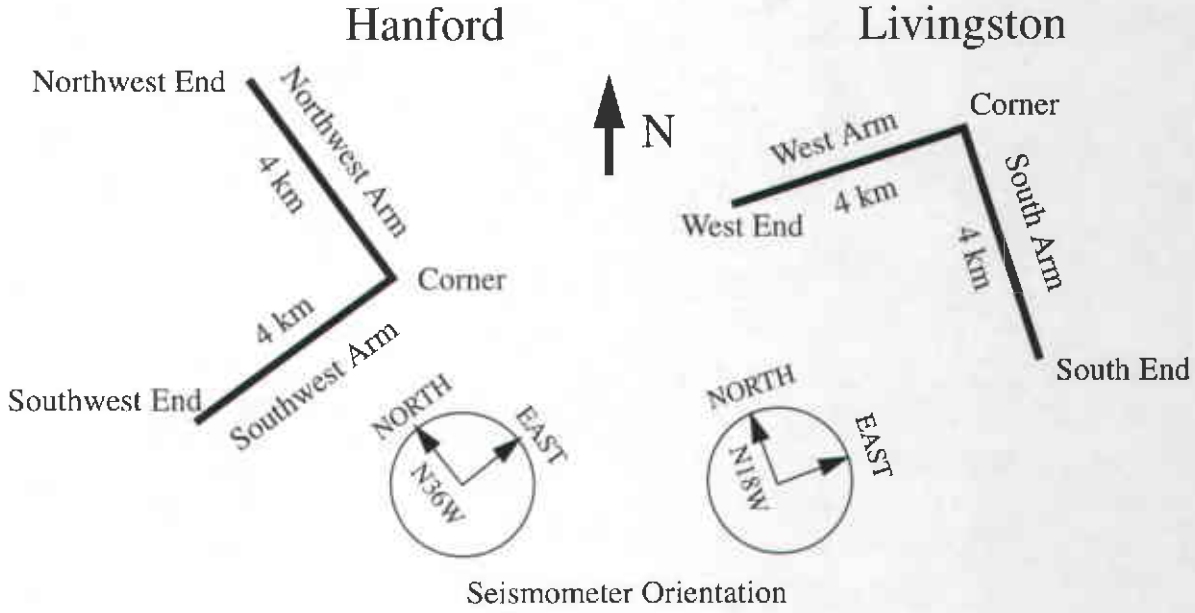

Figure 1. Orientation of seismometer components at LIGO sites at Livingston and Hanford.

The average of twelve one-hour displacement spectra for the vertical, "north", and "east" components at Livingston and Hanford are shown in Figure 2. The spectra from the three measurement locations (Corner and two Ends) are superimposed in each of the panels in Figure 2, and generally overlie each other between 0.1 and 1 Hz. The Livingston spectra exhibit a broad peak near 185 mHz, and the peak is higher on the horizontal components. At Hanford, the peak is much narrower and at lower frequency (near 125 mHz), and all three components have about the same amplitude. The noise amplitudes at Hanford are significantly smaller than those at Livingston across most of the frequency range shown. The Hanford spectra show a uniform decrease in amplitude from 0.2 to 1 Hz. The Livingston spectra show secondary peaks near 0.3 and 0.7 Hz, particularly on the vertical spectra.

Appendix A contains a set of color spectrograms that illustrate the temporal variation in the noise from 0.1 to 1 Hz.The spectrograms show the amplitude of ground velocity (as output by the seismometer) color-coded as a function of frequency and time. Spectra are taken from 180-s windows that are shifted 90 s. Each plot shows the spectra for a 24-hour period, when available. For the Hanford site, data from the 1994 deployment are shown from one day at each of the three measurement sites in addition to the 12-hour period in 1996 when the simultaneous measurements were taken.

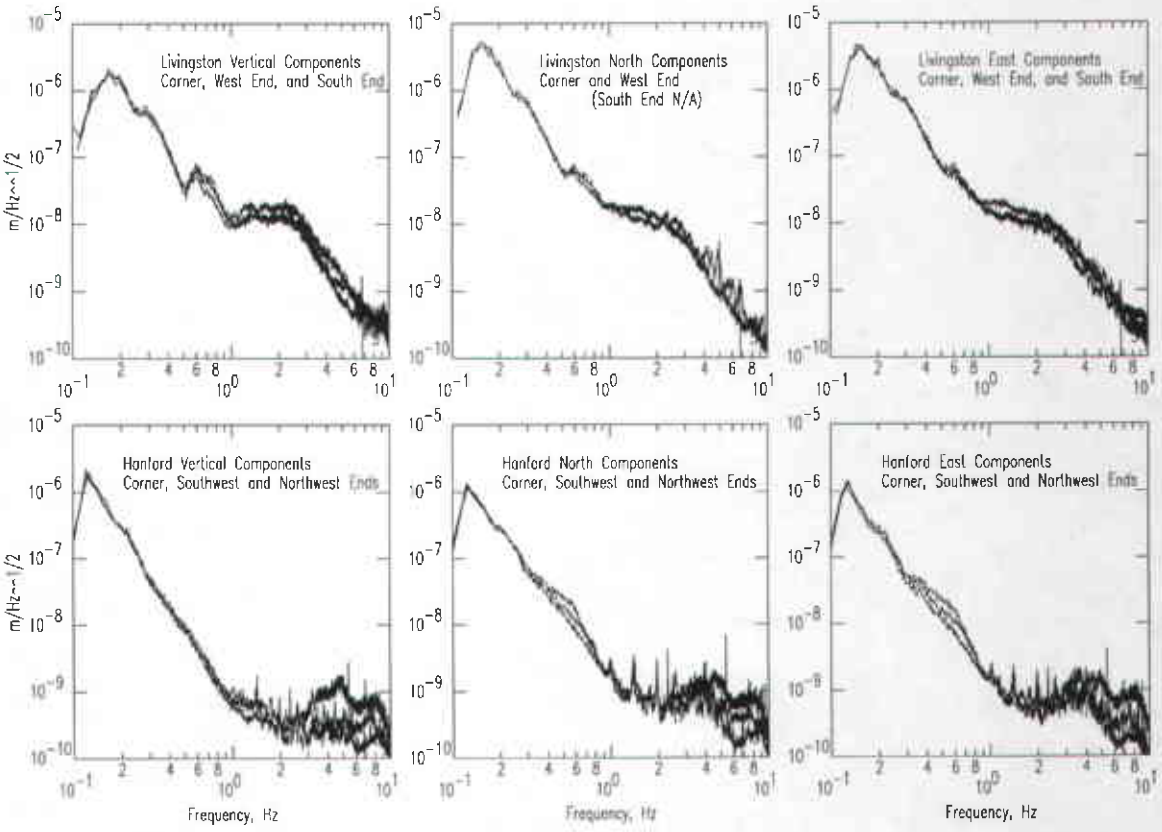

Figure 2. Amplitude spectra for Livingston and Hanford. Each spectrum is an average of 12 spectra computed from one-hour samples. Each plot overlays the spectra from the three measurement locations (Corner and two Ends) for parallel measurement directions (see Figure 1). Livingston spectra are shown in top row, Hanford spectra in bottom row.

3.0 Noise Model

Ambient seismic noise measured on land in the frequency range 0.1 - 1 Hz is usually dominated by a noise peak near 0.15 - 0.2 Hz, termed the "microseism" noise. Seismic array studies are consistent with a model of microseism noise generation that involves the interaction of ocean waves travelling in different or opposite directions. The interaction of the waves establishes a standing-wave pattern, and pressure fluctuations are then transmitted into the ocean floor. Seismic studies identify areas where different sets of ocean storm waves interact or where ocean storm waves reflect off of particular beaches. Three-component polarization and analysis of seismic array data indicate that microseismic noise is usually dominated by Rayleigh-wave propagation at velocities near the average crustal shear-wave velocity (typically 3.5 km/s), although higher-velocity body waves are also detected. It has been observed that the average microseism noise is higher in the northern latitudes during the first and fourth quarters of the year, when storm activity is more frequent and intense.

A wavenumber analysis of the microseism noise at Livingston and Hanford is described in Appendix B that is interpreted in terms of the distribution of source directions and propagation velocities. A summary of the wavenumber results for the frequency peak of microseism noise at Hanford (125 mHz) and at Livingston (185 mHz) is shown in Figure 3. At Hanford the dominant wave speeds are higher than 3 km/s at the frequency peak near 125 mHz, but at Livingston, the dominant wave speeds are less than 3 km/s at the frequency peak near 185 mHz. At Hanford, there are many periods when wave speeds are estimated near 6 km/s (and a few higher). At Livingston, the clusters of velocities near 1 km/s (at western and southeastern azimuths) are most frequently considered artifacts of the "beampattern" of the array.

The high wave-speed estimates at Hanford result from relatively small phase differences in the noise time series at the three measurement sites. The wavenumber results at Hanford typically imply seismic waves travelling at 3.5 km/s with a period of 8 seconds, corresponding to a wavelength of 28 km. This wavelength is 7 times longer than the 4 km arms of the L-shaped array formed by the LIGO measurement locations. For a sinusoidal wave travelling parallel to a 4-km arm, this leads to a 50-degree phase delay and will a produce a sinusoidal positional difference 15% smaller than the original input. In Figure 2, the azimuth histogram and polar plot for Hanford shows that the most frequently-observed directions of wave approach are nearly perpendicular to the Northwest Arm, and in this situation a larger reduction in differential motion results on this arm.

The wavenumber results at Livingston imply a wave velocity near 2 km/s at the frequency peak near185 mHz, corresponding to a wavelength near 11 km. If these waves were travelling parallel to one of the arms, a phase delay of 135 degrees would result. However, the azimuth histogram and polar plot in Figure 2 show that the dominant wave direction is from the north-northeast, which practically bisects the arms' orientations. In this situation, a phase delay of just over 90 degrees results on both arms and the differential motion will be just over 40% larger than the original input.

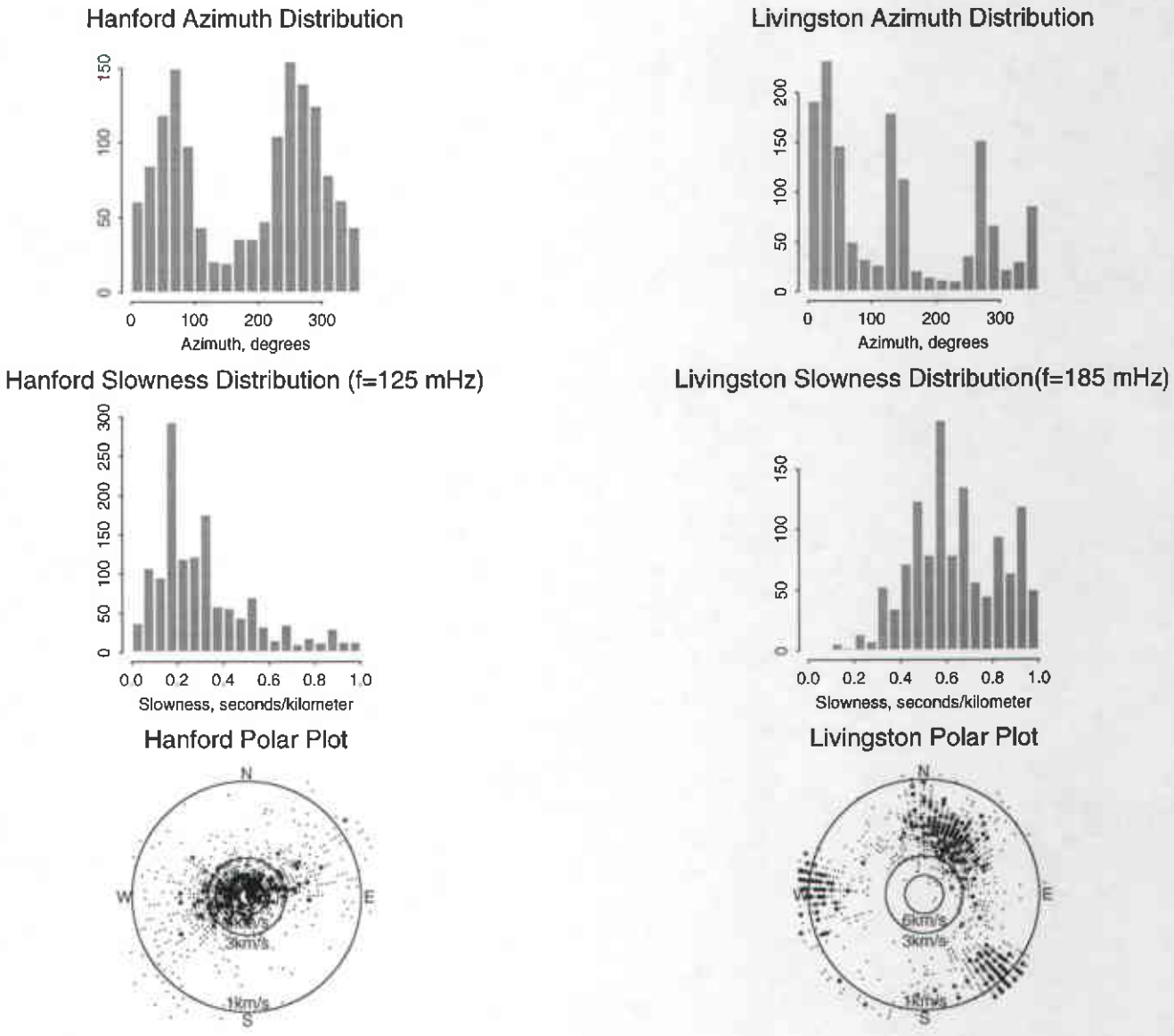

Figure 3. Summary of wavenumber analysis. The determination of apparent velocity and direction of the peak microseismic noise is described in Appendix B. At Hanford, the propagation velocity is most frequently determined to be faster than 3 km/s. At Livingston, the propagation velocity is most frequently determined to be slower than 3 km/s. The lower propagation velocity at Livingston creates artificial concentrations at velocities near 1 km/s at western and southeastern azimuths (due to the beam-pattern effect). The larger symbols in the polar plots (bottom) correspond to the largest coherent noise amplitudes (upper 25th percentile) measured.

4.0 Differential Motions

The r.m.s. difference in position of the Corner and End stations is determined in three one-octave frequency bands, using a sample length that corresponds to one cycle of the lowest frequency in the band or two cycles of the highest frequency, as shown in the table below. The effect of the band-pass filters on a sample spectrum from Livingston is shown in Figure 4.

Frequency Band (Hz)	Sample Length (s)	Number of Samples
0.1 - 0.25	8	5400
0.25 - 0.5	4	10800
0.5 - 1.0	2	21600

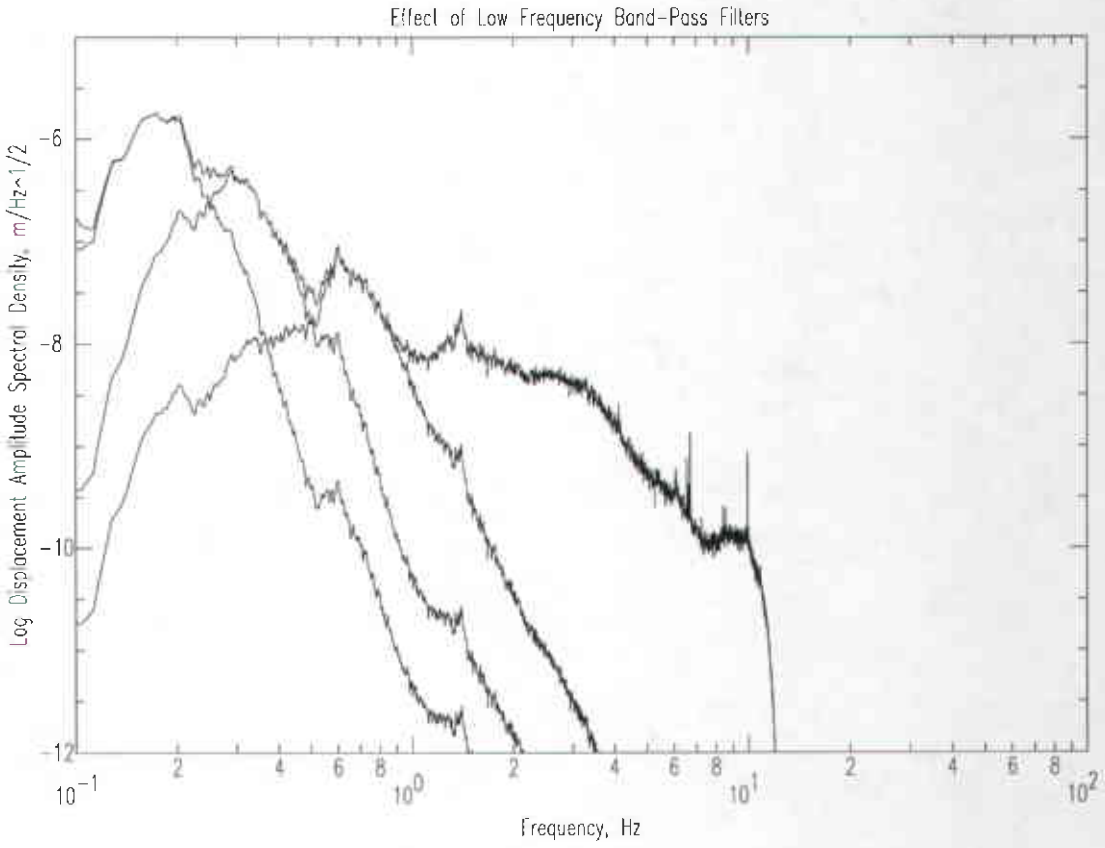

Figure 4. Effect of band-pass filters on an example spectrum. Spectra are averages of 39 spectra taken within a one-hour time sample at Livingston. Plot superimposes spectra from the unfiltered and three band-passed time series. The filters are two-pole Butterworth filters that operate twice (forward and backwards through the time series) to eliminate phase shift. Filter frequency limits are 100-250 mHz, 250-500 mHz, and 500-1000 mHz. The effect of the anti-alias filter used to decimate data to 25 samples/second is seen at 12.5 Hz.

The lowest frequency band includes the peak amplitude of the ambient noise spectra at the Hanford and Livingston LIGO sites that were described in the previous sections. The processing of the data for calculating the position differences from the recorded signals is similar to that used for the wavenumber analysis, using one-hour segments of 25 samples/second time series that have had the first and last 0.5% tapered to zero to avoid transient effects (18 s of data at the start and end of each hour are affected). Note that this tapering will affect the extreme tail of the distribution of small displacements but does not significantly affect the distribution of displacements above 99% probability of exceedance (it can randomly remove up to 1% of the population of higher displacements).

The tapering above was also necessary to eliminate transients from the conversion of the 30-s seismometer to be identical to the two 20-s seismometers. The gain factor for each time series was applied to obtain ground velocity from the digitally-recorded seismometer outputs. Band-pass filters were applied to each one-hour time series, and then the time series were integrated to obtain ground displacement from the filtered velocity time series.

The Corner-to-End difference between the displacement time series was determined for each component of the seismometer systems. The vertical difference corresponds to a vertical tilting of the two arms. The north difference corresponds to an arm-parallel displacement or strain of the Northwest Arm at Hanford or the South Arm at Livingston (see Figure 1), and rotation (about a vertical axis) of the Hanford Southwest Arm or the Livingston West Arm. The east difference similarly corresponds to an arm-parallel displacement of the Southwest Arm at Hanford or the West Arm at Livingston and rotation of the corresponding perpendicular arms.

Comparison of differential motions to independent motions. Figures 5 to 10 show histograms of the ratio of the r.m.s. displacement differences to the r.m.s. of the two contributing independent motions. At the bottom of each histogram are two triangles marking the mean and median value of the ratios. The value of this ratio can range from 0 to 2, if the two displacement time series are identical or opposite. The r.m.s. amplitude of the difference between two random time series is expected to have a ratio of 1.4 (assuming equal r.m.s. amplitudes of the original signals). The difference between two sinusoidal signals with a phase difference of 90 degrees will also have this ratio.

The distributions of ratios for the vertical motions at Livingston are shown in Figures 5. In the two higher frequency bands (250-500 and 500-1000 mHz), the mean and median values are near the value expected from the difference between two un-correlated time series. The ratios for the lowest frequency band (100-250 mHz), where the motions are largest, are slightly higher than this value. This is consistent with the results of the wavenumber analysis that was conducted within this frequency range. The wavenumber analysis of the vertical components most frequently detected phase differences near 100 degrees between the Corner and the two Ends.

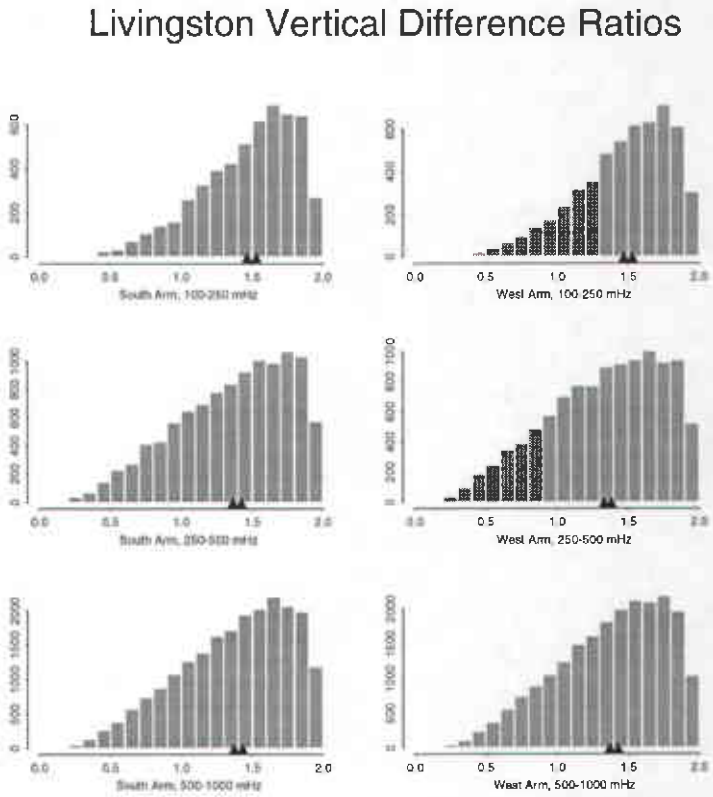

Figure 5. Histograms of End-Corner difference ratios for Livingston r.m.s. vertical component of ambient ground motion.

The distributions of ratios for the horizontal motions at Livingston are shown in Figures 6 and 7. The east-component distributions are similar to the vertical component, and the north component distributions are similar except for a slightly increased ratio (up to 1.6) in the low- and intermediate-frequency bands for the West Arm (this motion is perpendicular to this arm or a rotation of the arm). Data from the north component at the South End was not available during this time period.

Figure 8 shows that at Hanford, significant reductions in differential motion result, particularly for lower frequencies and for the Northwest Arm. This is consistent with the wavenumber analysis that showed small phase differences due to high propagation velocities across the array. The reduction of differential motion relative to independent motion is stronger on the Northwest Arm, which is perpendicular to one of the principal azimuths (from the northeast) determined in the wavenumber analysis. Figures 9 and 10 show the ratios for the north and east components, which have similar distributions. Along the Southwest Arm, there is a significant reduction in differential motion only for the lowest frequency band, but the ratios determined for the intermediate and higher bands are close to 1.4.

Livingston North Difference Ratios

Data from South End was not available during this time period.

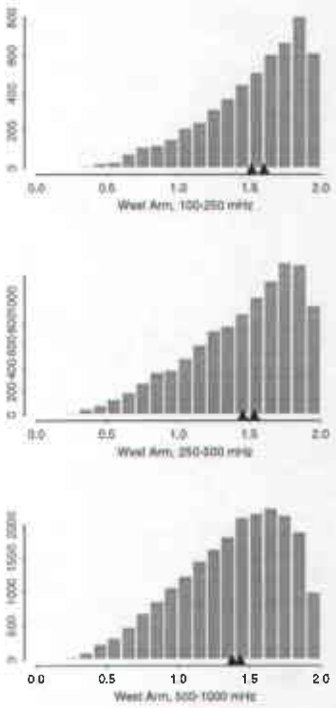

Figure 6. Histograms of End-Corner difference ratios for Livingston r.m.s. north component of ambient ground motion.

Livingston East Difference Ratios

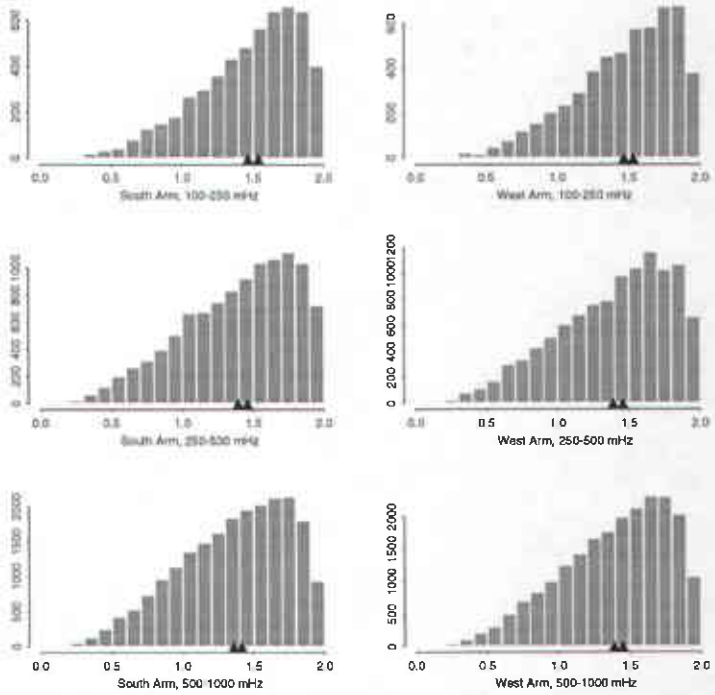

Figure 7. Histograms of End-Corner difference ratios for Livingston r.m.s. east component of ambient ground motion.

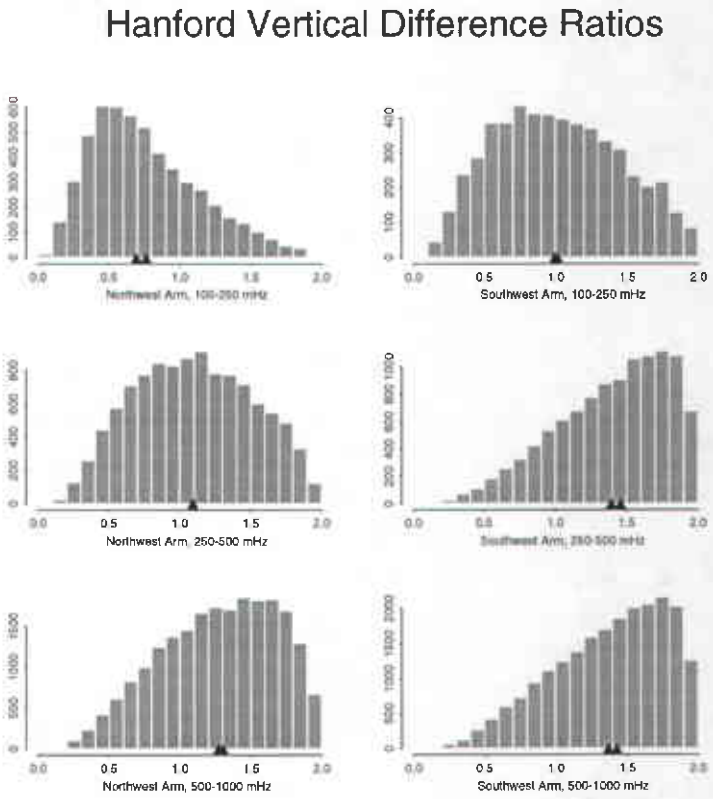

Figure 8. Histograms of End-Corner difference ratios for Hanford r.m.s. vertical component of ambient ground motion.

Differential Motion Histograms. The set of twelve figures at the end of this report, Figures 11 through 22, show the cumulative exceedances of r.m.s. differential displacements in the three frequency bands and set of sampling windows used above. Each figure displays the cumulative distribution of r.m.s. displacement for each of the contributing independent motions and their differences, for each of the three frequency bands. The histograms have a resolution of 0.05 log units. A complete description of the differential motions in three directions (vertical tilting, arm-parallel stretching, and horizontal rotation) is provided for Livingston (Figures 11 to 16) and Hanford (Figures 17 to 22). For both sites, the largest displacements are found in the 100-250 mHz band.

The r.m.s. amplitude of the independent motions at the Corner and either End are usually within 0.05 log units (about 12%) of each other. However, independent r.m.s. motions for the vertical components at Livingston and the horizontal components at Hanford in the frequency band 0.5-1.0 Hz show a variation of approximately 0.15-0.20 log units. This is consistent with the higher variability of the spectra in this frequency range shown in Figure 2.

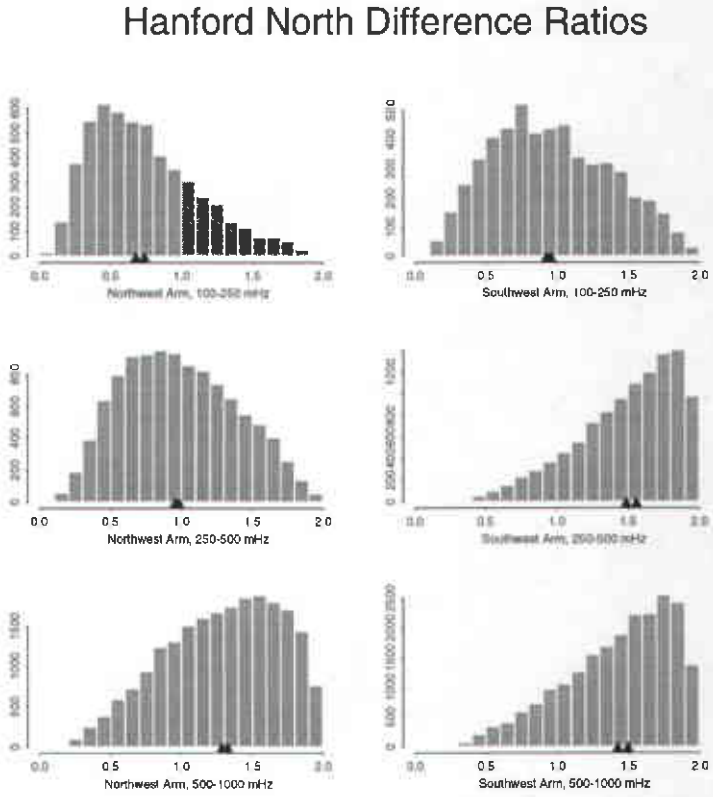

Figure 9. Histograms of End-Corner difference ratios for Hanford r.m.s. north component of ambient ground motion.

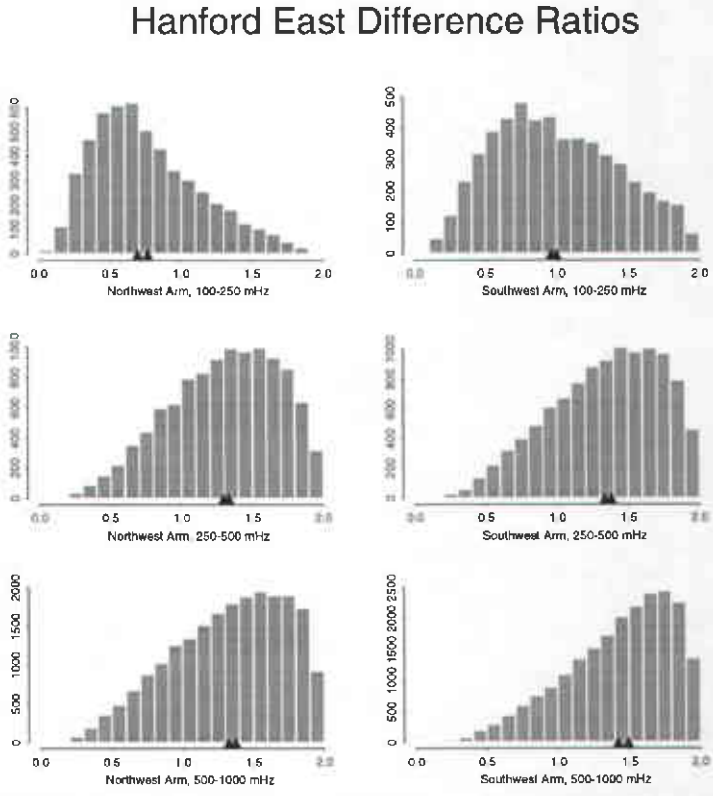

Figure 10. Histograms of End-Corner difference ratios for Hanford r.m.s. east component of ambient ground motion.

At Livingston differential displacements exceed 10^{-6} m approximately 90% of the time for the horizontal motions, and approximately 30% of the time for vertical motions in the low-frequency band. Differential motions are larger than independent motions in all frequency bands. In the lowest frequency band (100-250 mHz), this increase is 40-60%, in agreement with the distribution of ratios in Figures 5-7. In the highest frequency band (500-1000 mHz) at occurrence rates below 1%, the plots show the effect of an earthquake (a magnitude 5 event from southern Mexico) that occurred during the 12-hour period analyzed. This earthquake's ground motion had a greater effect on the horizontal motions.

At Hanford, differential displacements rarely exceed 10^{-6} m in the low-frequency band. The differential motion is reduced relative to independent motion in the low-frequency band, especially for the Northwest Arm where the reduction is 30%. Higher signal coherence and smaller phase differences along this arm were detected by the wavenumber analysis. The Southwest Arm was oriented parallel to the dominant microseism propagation directions and so the phase differences on this arm were larger. The correlation progressively degrades for the mid- and high-frequency bands, and the increase of differential motion relative to independent motion attains values near the expected value from completely un-correlated signals.

5.0 Conclusion

The microseism noise, peaked in amplitude near 125 mHz at Hanford and near 185 mHz at Livingston, produces the largest displacements at the two LIGO sites. This noise is expected to be produced from oceanic or coastal areas and to propagate at velocities near the average shear-wave velocity of the earth's crust, approximately 3.5 km/s. This model should produce a reduction or at worst a slight increase in the amplitude of differential motions between the End stations and the Corner because of the long wavelengths implied. However, at both Hanford and Livingston, the observed phase relationships between measurement sites differ from this model.

At Hanford, wavenumber analysis in the 100-150 mHz band most frequently indicates velocities of 3.5 km/s and higher, from a range of western azimuths that would be appropriate for sources in the Pacific ocean or along the coast. But there are also many periods when a northeast azimuth is determined. The periods when a northeast or southwest azimuth is determined result in coherent motions at the Northwest End and Corner, which significantly reduces the average differential motion along this arm. The high average velocities produce a reduction of Corner-to-End differential motion on both arms relative to that expected from un-correlated motions. This reduction is most effective in the frequency range that the peak microseism amplitudes are observed, but the microseism signals become progressively less coherent at higher frequencies.

At Livingston, the phase relationships between the Corner and Ends indicate unusually slow velocities (near 2 km/s) for propagation of microseism noise, and a direction of propagation that does not correspond to sources near coasts or in the oceans. The slow velocity may result from a thick layer of sediments, but the velocity structure of this region is not well known. If velocities slower than 1 km/s are possible for these low-frequency waves,

other azimuths are also possible. It is also possible that patterns of interfering waves frequently establish stable phase relationships between the Corner and Ends that do not necessarily correspond to the actual propagation direction of the components of the wave field. Although the results at Livingston indicate larger phase differences between the Ends and the Corner than expected, they only modestly increase the average ratio of differential motions to independent motions relative to that expected for completely random signals (a ratio of 1.6 compared to the expected ratio of 1.4).

The difficulty in characterizing the propagation modes of microseism noise from 0.1 to 1 Hz arises because the array geometry is suitable only for wavelengths significantly longer than the spacing between measurement locations. In order to determine whether multiple signals might be present in the wave field, more than three measurement locations must be occupied. The anomalously slow wave velocities implied by the wavenumber analysis at Livingston suggest that the propagation characteristics of the microseismic noise there may not be consistent with previous characterizations of this noise as fast, long-wavelength Rayleigh waves.

Cumulative histograms of differential motion along the arms of the Hanford LIGO site indicate that the 90th-percentile differential displacement has an amplitude of approximately 4×10^{-7} m in the 100-250 mHz band. This compares to an approximate 90th-percentile value at the Livingston LIGO site on the order of 4×10^{-6} m. These values correspond to strains, rotations, or tilts of the 4-km arms by 0.1 and 1.0 parts per billion for the Hanford and Livingston LIGO sites, respectively.

Note added in proof: The data from the Livingston South End north component during the time period analyzed in this report were later found to be in error. It is recommended that the differential motion of the north components along the West Arm be used as a surrogate for those along the South Arm, because the dominant direction of microseism propagation is oriented at 45 degrees to the two arms. Data from an earlier or later time period are available for a revised analysis.

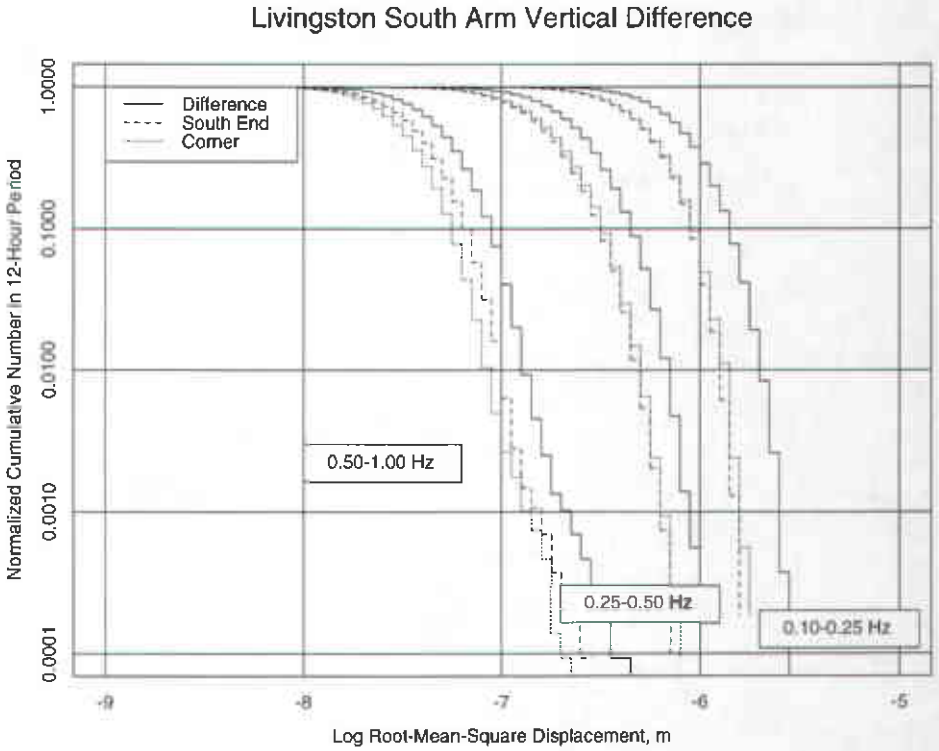

Figure 11. Cumulative distribution of independent and differential r.m.s. vertical-component displacements at Livingston South Arm.

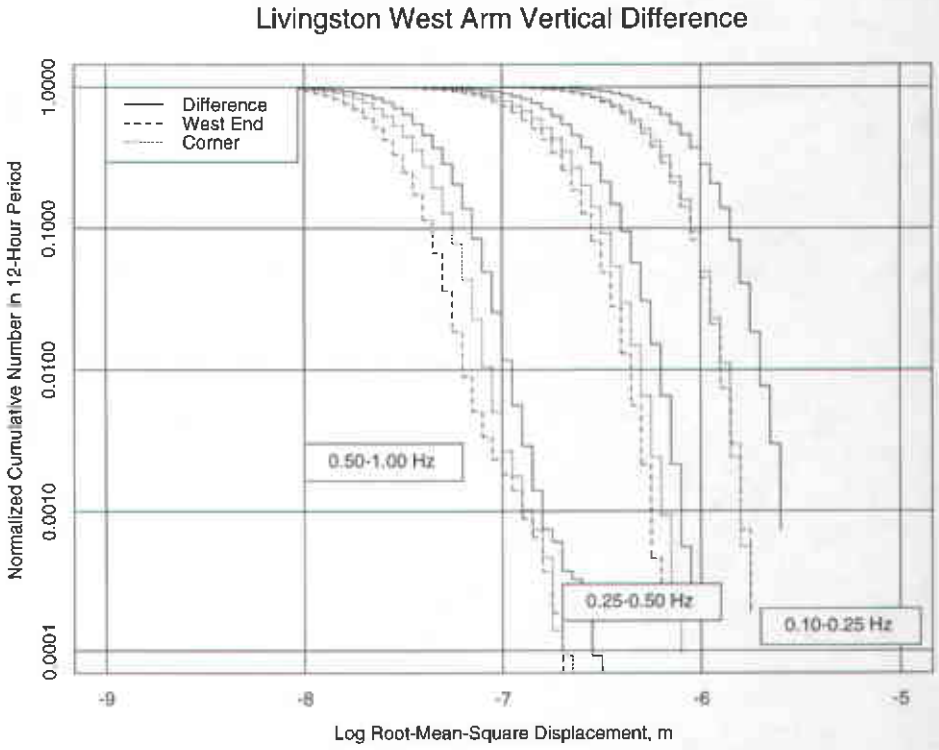

Figure 12. Cumulative distribution of independent and differential r.m.s. vertical-component displacements at Livingston West Arm.

Data from the north component
at the South Arm was not
available during this time period.

Figure 13. Cumulative distribution of independent and differential r.m.s. north-component displacements at Livingston South Arm.

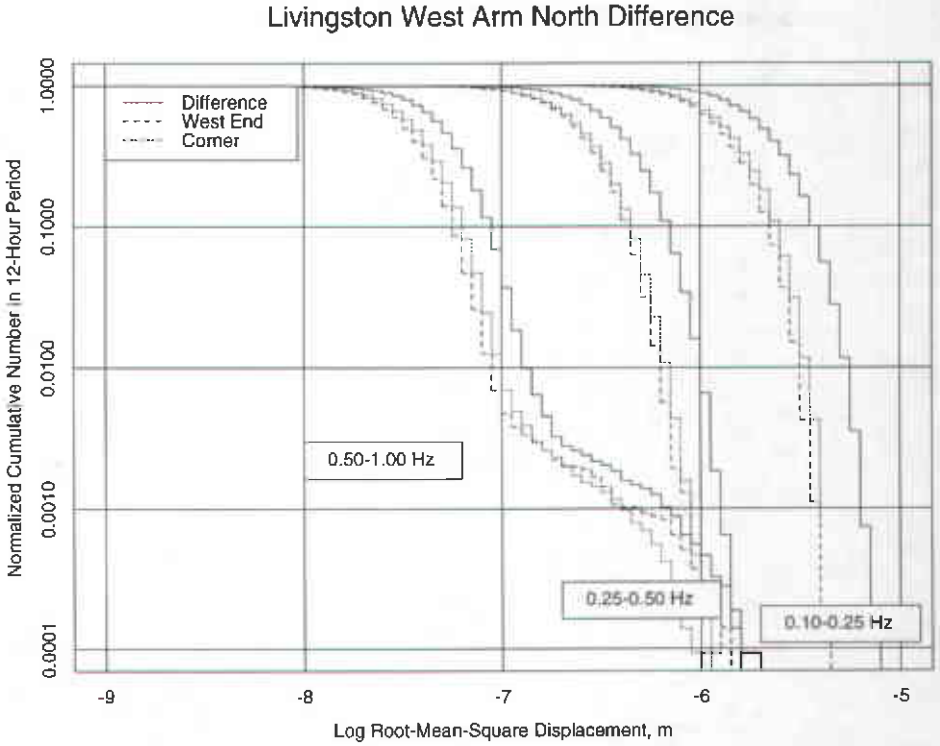

Figure 14. Cumulative distribution of independent and differential r.m.s. north-component displacements at Livingston West Arm.

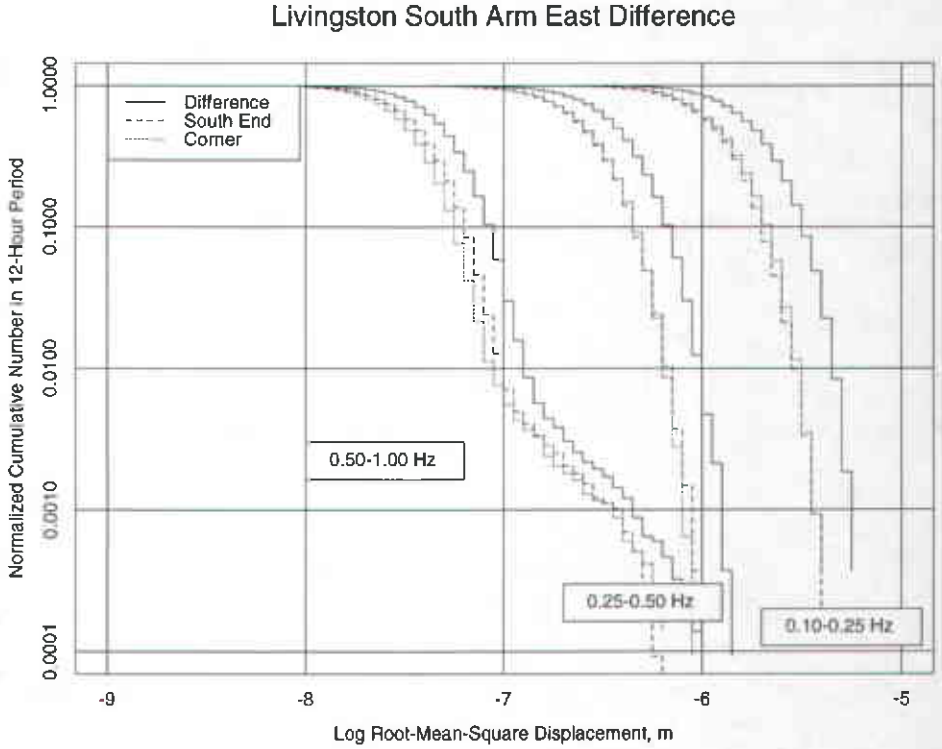

Figure 15. Cumulative distribution of independent and differential r.m.s. east-component displacements at Livingston South Arm.

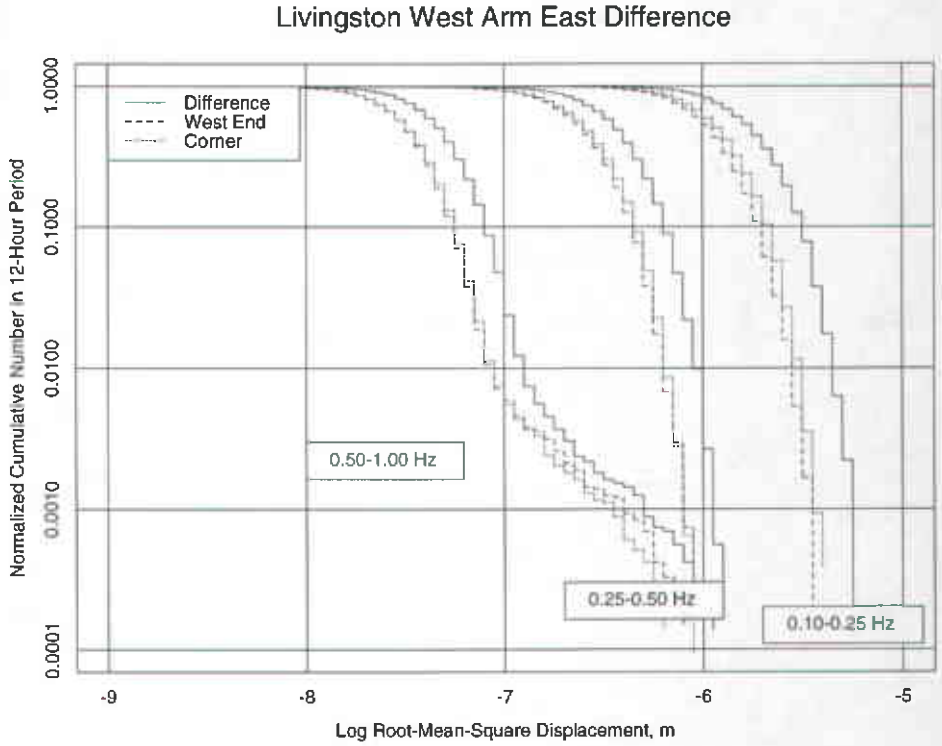

Figure 16. Cumulative distribution of independent and differential r.m.s. east-component displacements at Livingston West Arm.

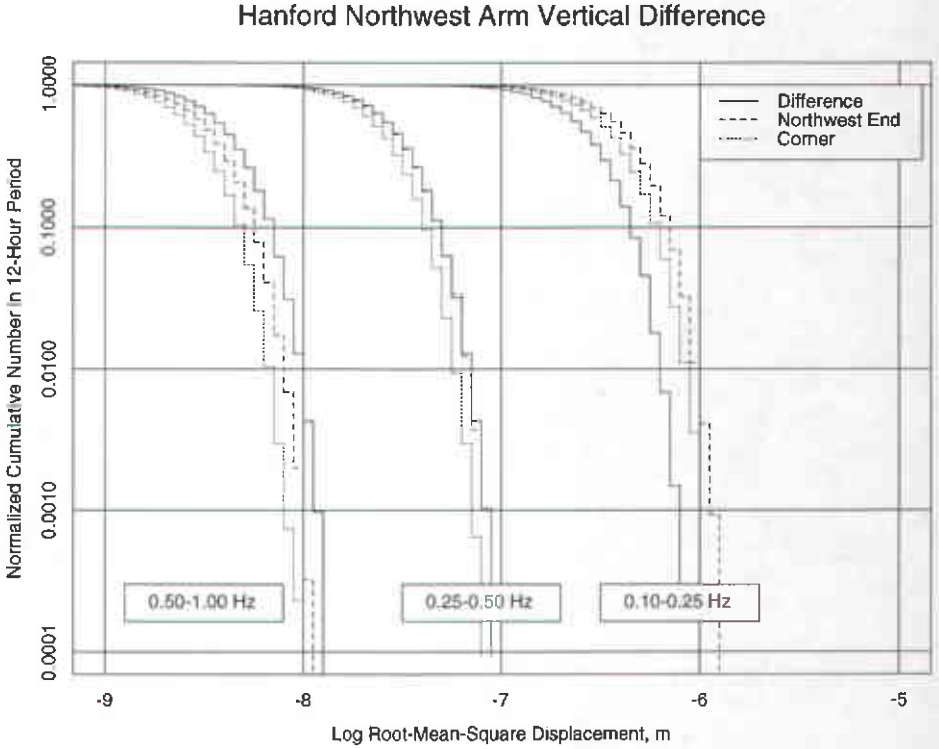

Figure 17. Cumulative distribution of independent and differential r.m.s. vertical-component displacements at Hanford Northwest Arm.

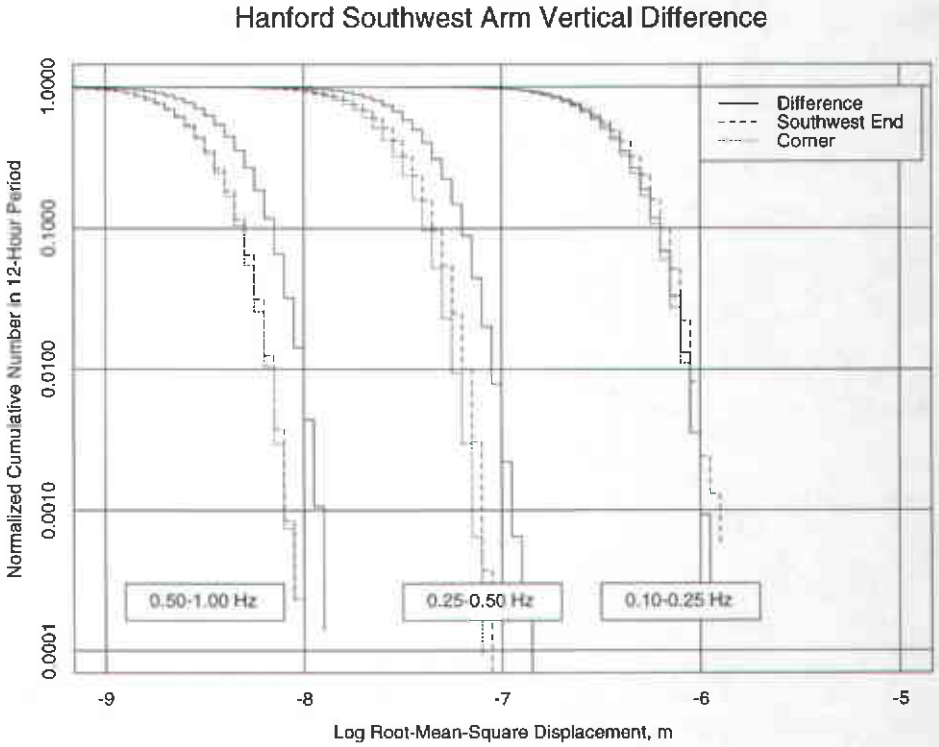

Figure 18. Cumulative distribution of independent and differential r.m.s. vertical-component displacements at Hanford Southwest Arm.

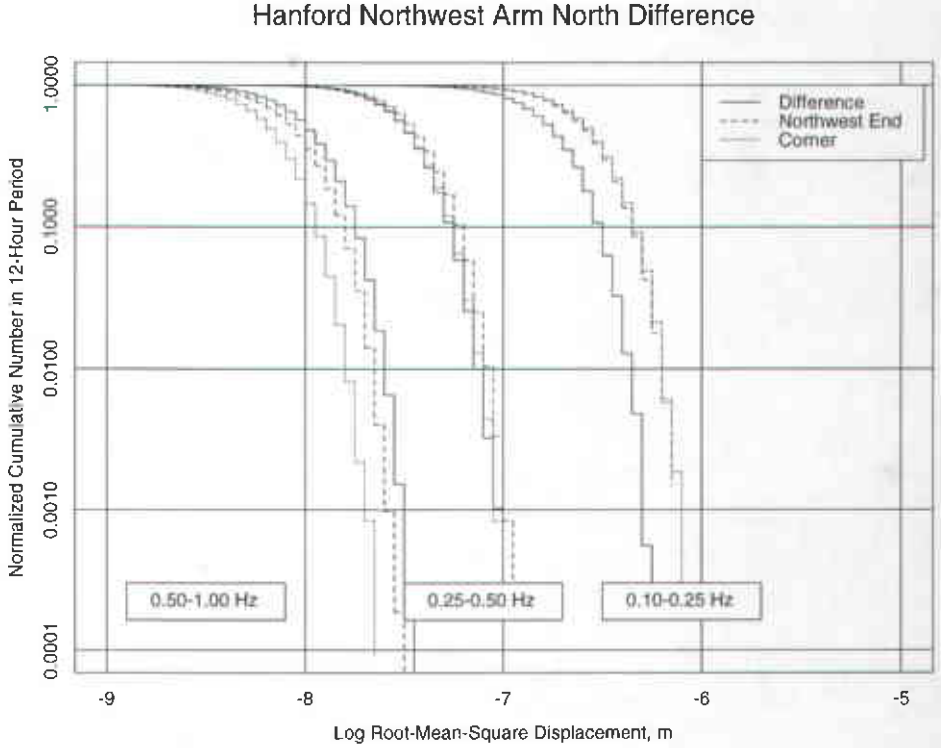

Figure 19. Cumulative distribution of independent and differential r.m.s. north-component displacements at Hanford Northwest Arm.

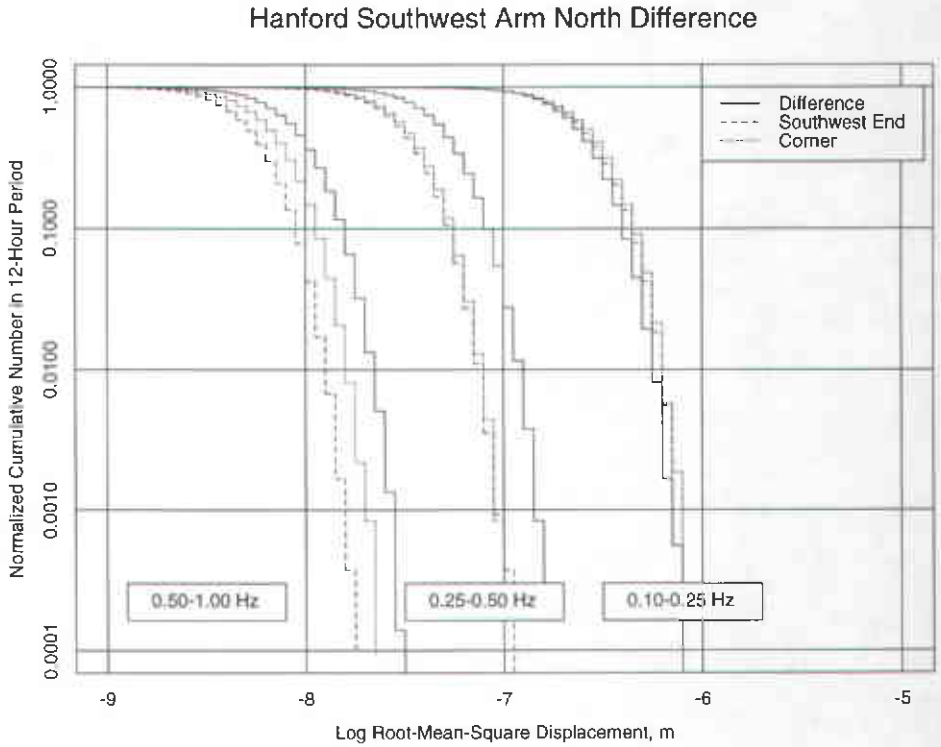

Figure 20. Cumulative distribution of independent and differential r.m.s. north-component displacements at Hanford Southwest Arm.

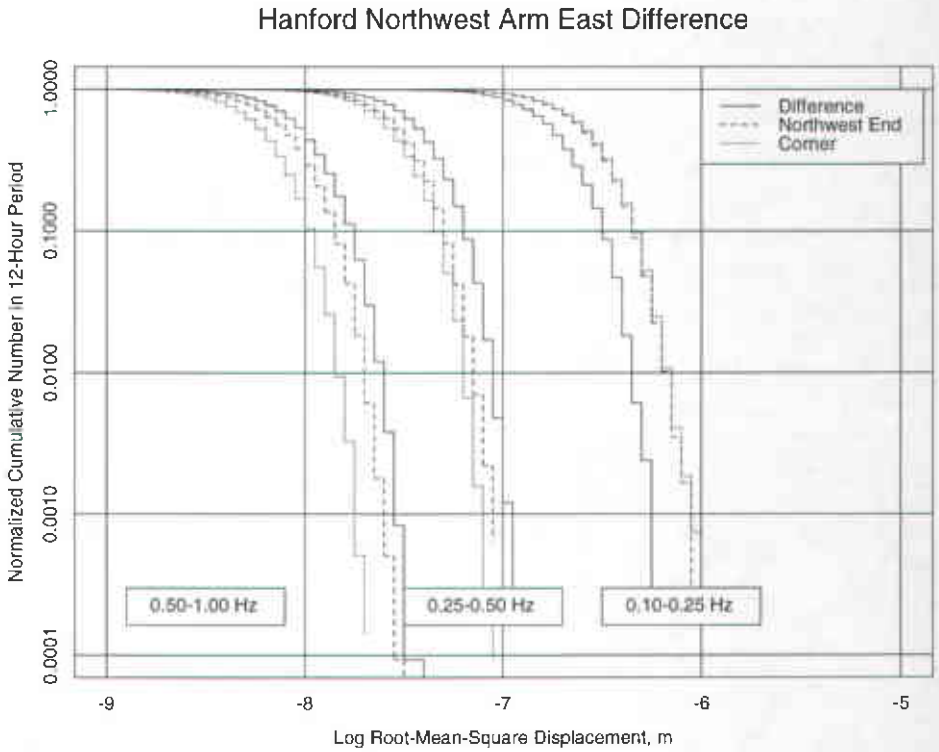

Figure 21. Cumulative distribution of independent and differential r.m.s. east-component displacements at Hanford Northwest Arm.

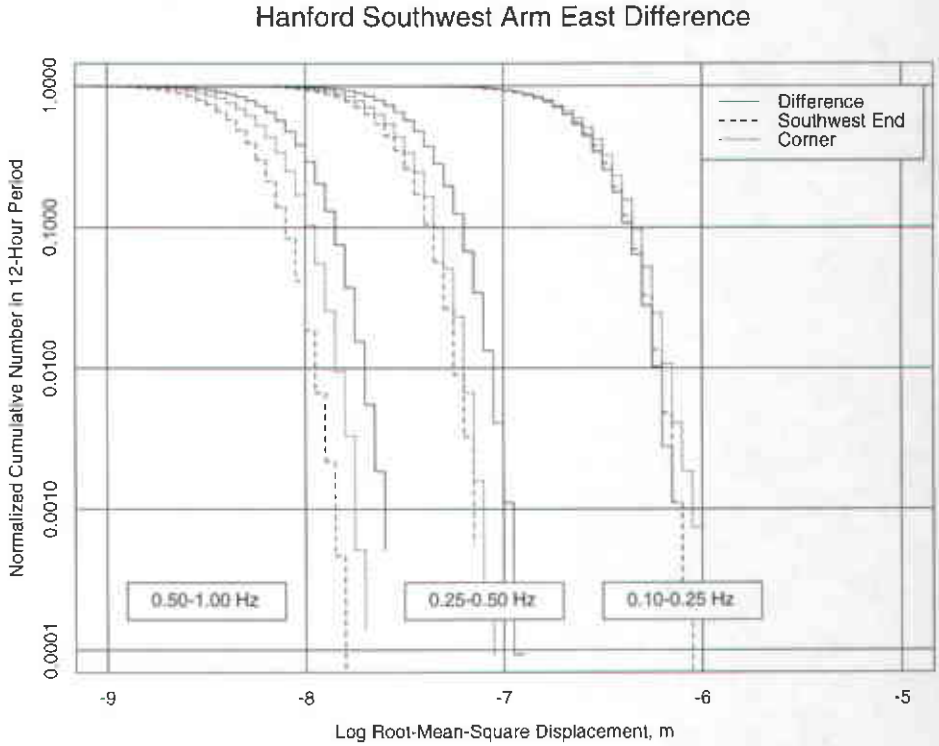

Figure 22. Cumulative distribution of independent and differential r.m.s. east-component displacements at Hanford Southwest Arm.

Appendix A

Color Spectrograms 0.1 to 1.0 Hz

LIVINGSTON 1995:

Corner	Vertical Component	Day 301
South End	Vertical Component	Day 301
West End	Vertical Component	Day 301
Corner	Vertical Component	Day 302
South End	Vertical Component	Day 302
West End	Vertical Component	Day 302
Corner	Vertical Component	Day 303
South End	Vertical Component	Day 303
West End	Vertical Component	Day 303
Corner	Vertical Component	Day 304
South End	Vertical Component	Day 304
West End	Vertical Component	Day 304
Corner	Infrasound Channel	Day 301
Corner	Infrasound Channel	Day 302
Corner	Infrasound Channel	Day 303
Corner	Infrasound Channel	Day 304

HANFORD 1996:

Corner	Vertical Component	Day 005
Northwest End	Vertical Component	Day 005
Southwest End	Vertical Component	Day 005

HANFORD 1994:

Northwest End	Vertical Component	Day 331
Southwest End	Vertical Component	Day 338
Southwest End	Infrasound Channel	Day 338
Corner	Vertical Component	Day 345

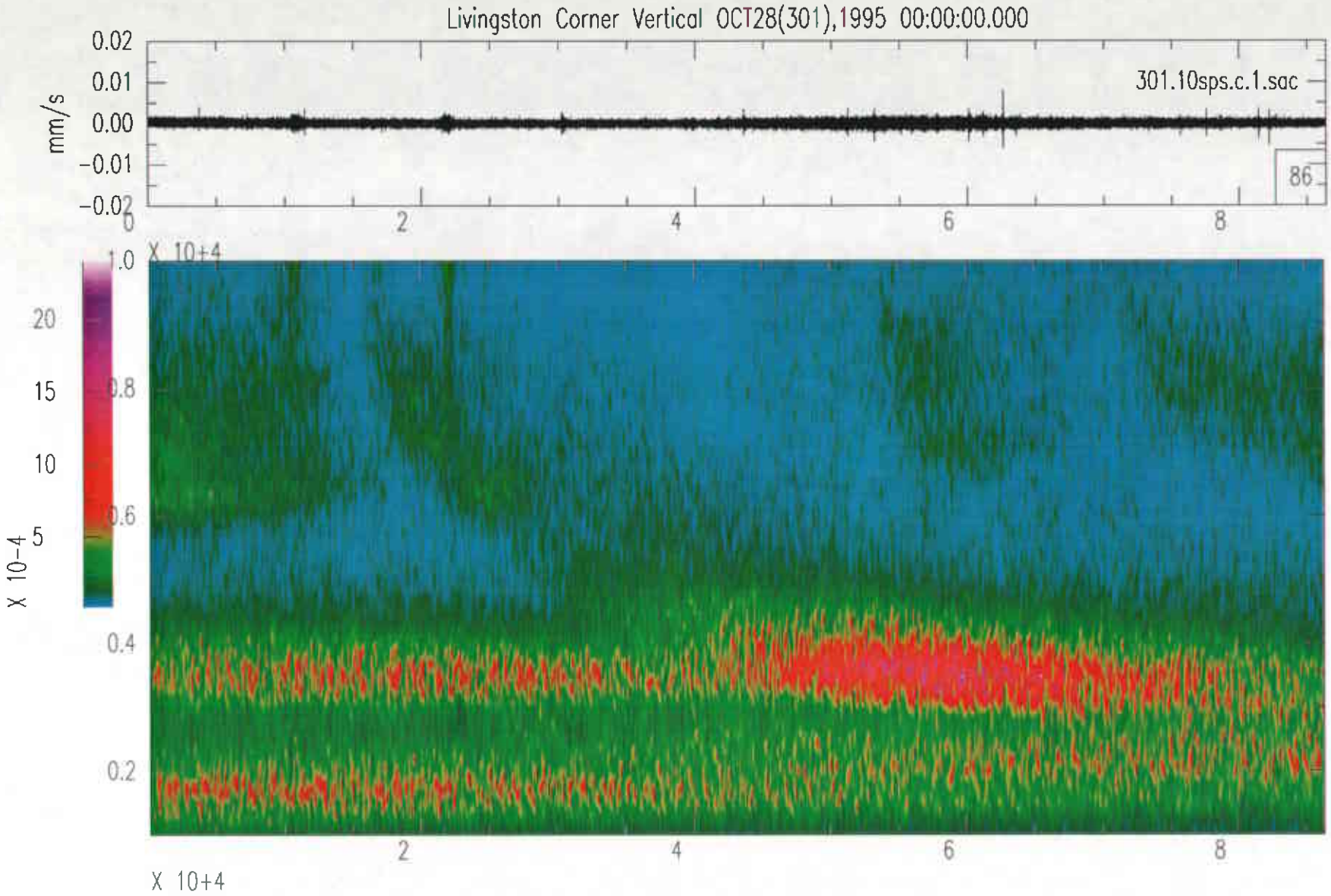
Livingston Corner Vertical OCT28(301),1995 00:00:00.000
301.10sps.c.1.sac
86
mm/s
0.02
0.01
0.00
-0.01
-0.02
0
2
4
6
8
X 10+4
1.0
0.8
0.6
0.4
0.2
20
15
10
5
X 10-4
2
4
6
8
X 10+4

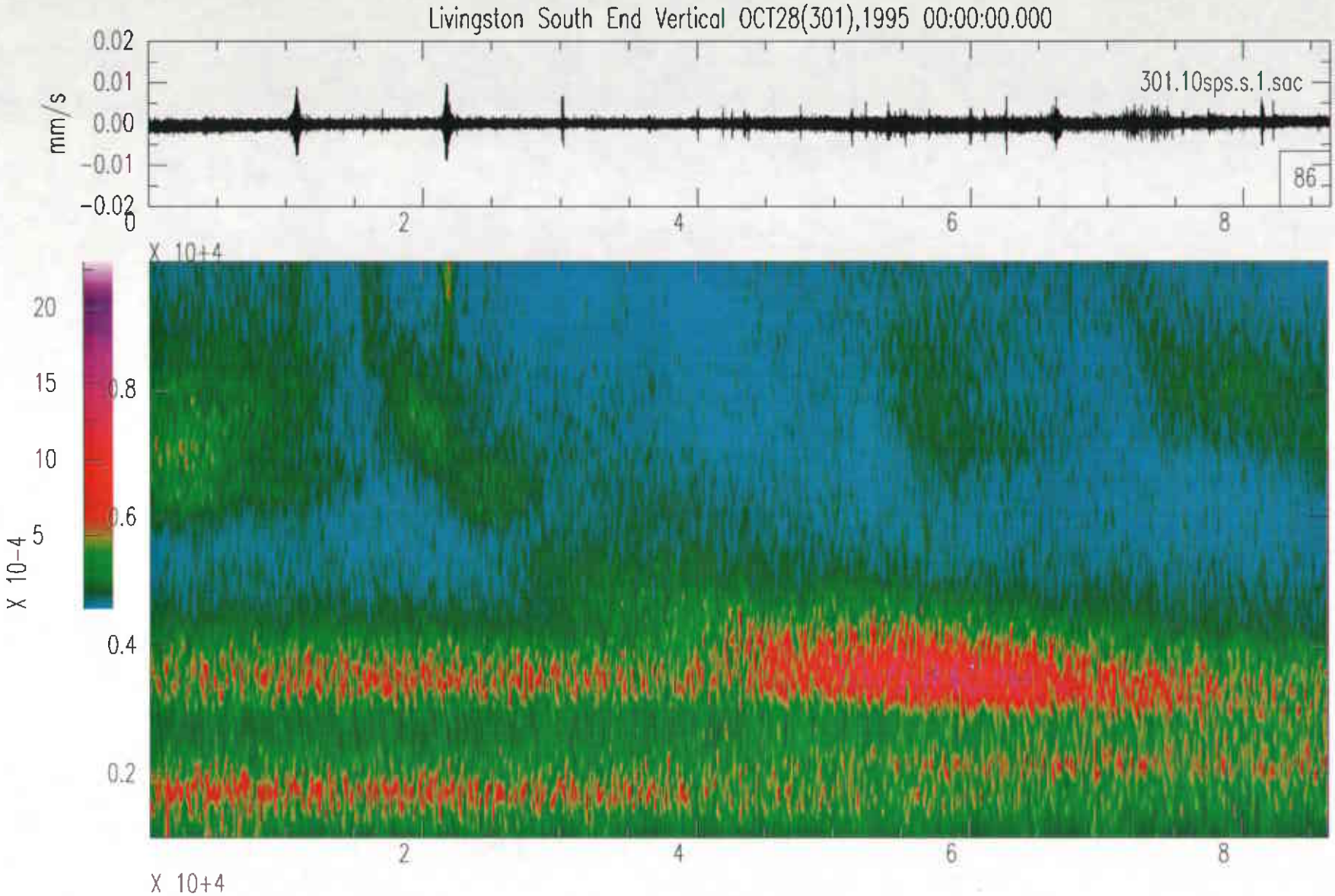
Livingston South End Vertical OCT28(301),1995 00:00:00.000
301.10sps.s.1.sac
86
mm/s
0.02
0.01
0.00
-0.01
-0.02
0
2
4
6
8
X 10+4
20
15
10
5
X 10-4
0.8
0.6
0.4
0.2
2
4
6
8
X 10+4

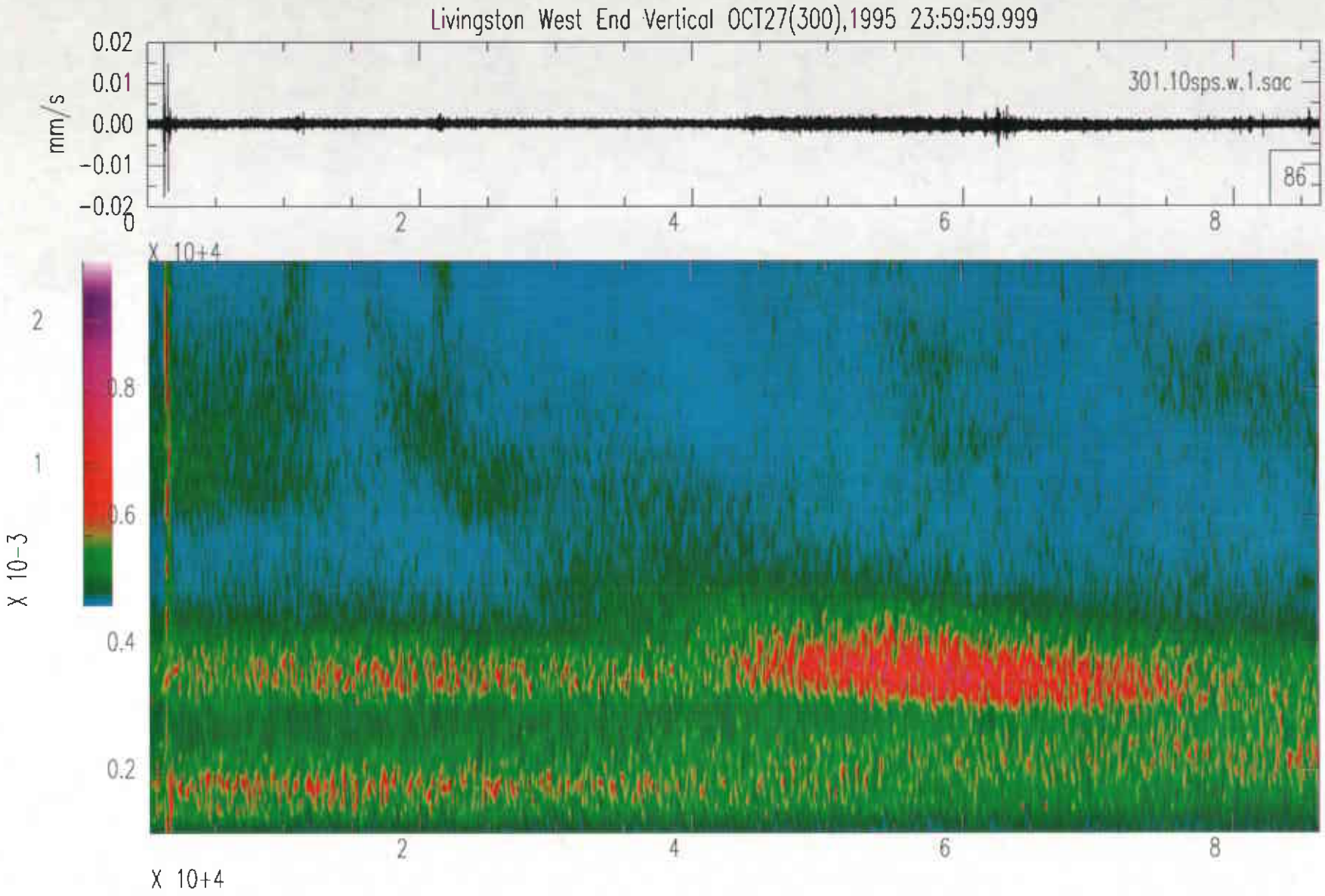
Livingston West End Vertical OCT27(300),1995 23:59:59.999
301.10sps.w.1.sac
86
mm/s
0.02
0.01
0.00
-0.01
-0.02
0
2
4
6
8
X 10+4
X 10-3
2
1
0.8
0.6
0.4
0.2
2
4
6
8
X 10+4

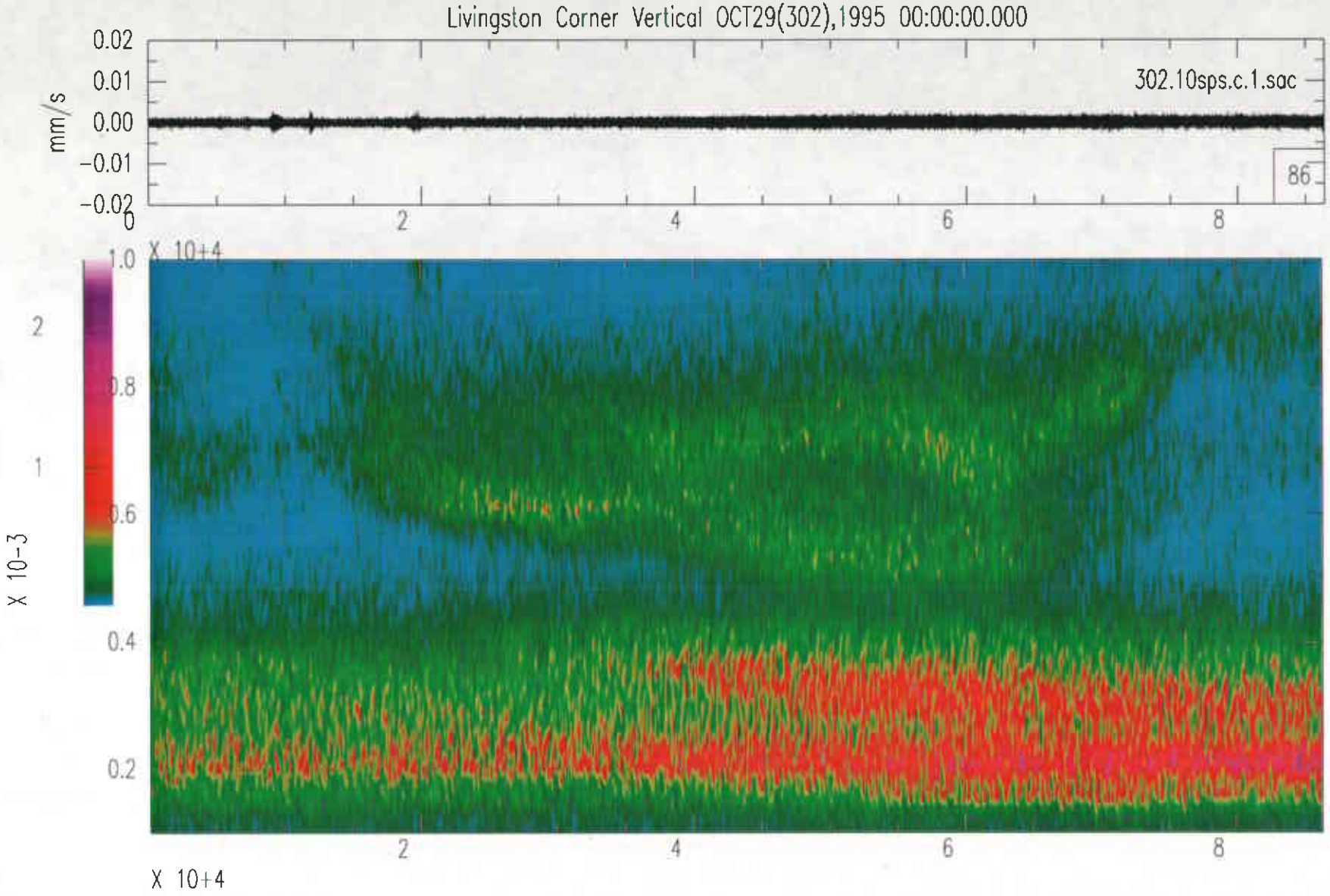
Livingston Corner Vertical OCT29(302),1995 00:00:00.000
302.10sps.c.1.sac
86
mm/s
0.02
0.01
0.00
-0.01
-0.02
0
2
4
6
8
X 10+4
1.0
0.8
0.6
0.4
0.2
X 10-3
2
1
X 10+4

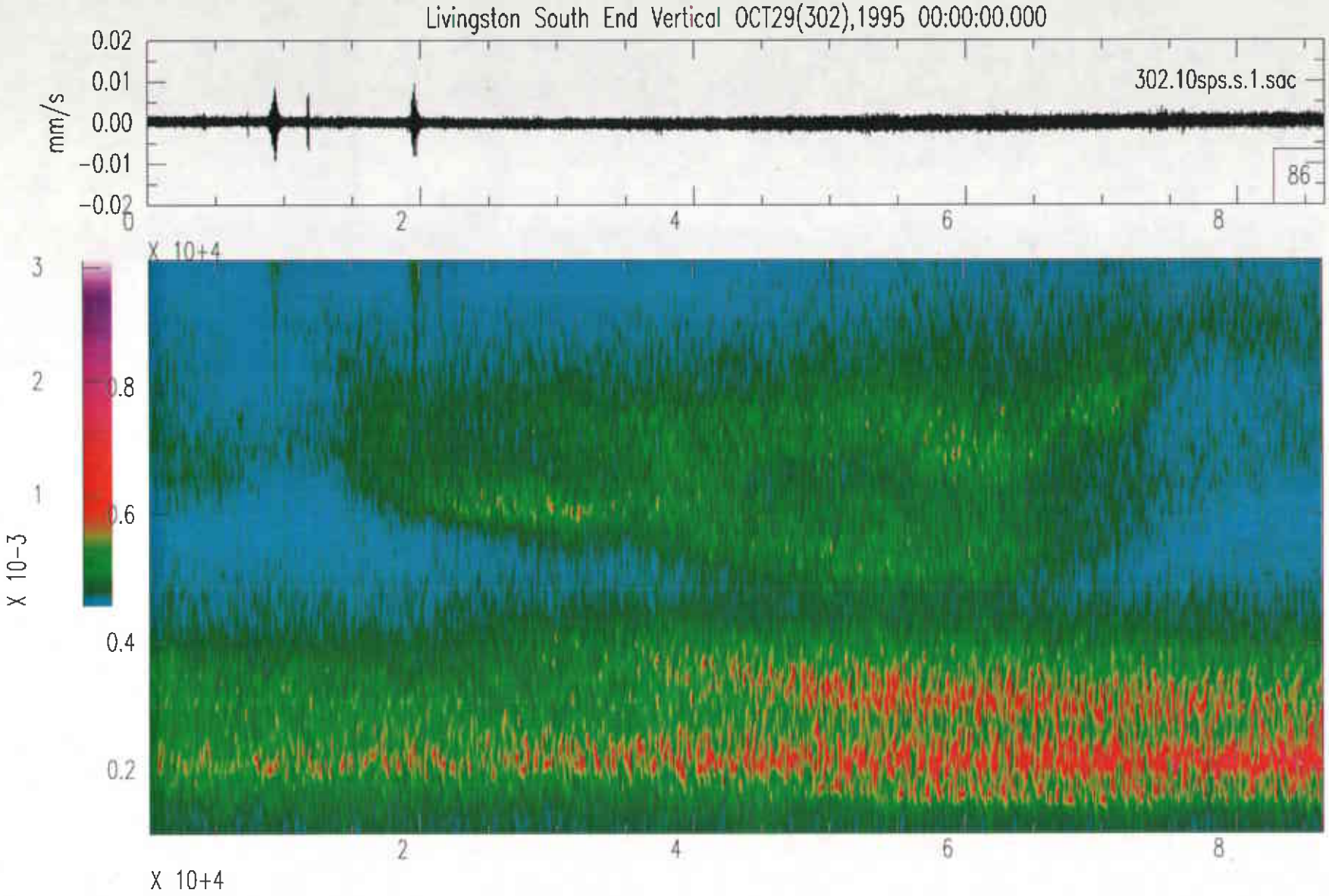
Livingston South End Vertical OCT29(302),1995 00:00:00.000
302.10sps.s.1.sac
86
mm/s
0.02
0.01
0.00
-0.01
-0.02
0
2
4
6
8
X 10+4
3
2
1
X 10-3
0.8
0.6
0.4
0.2
2
4
6
8
X 10+4

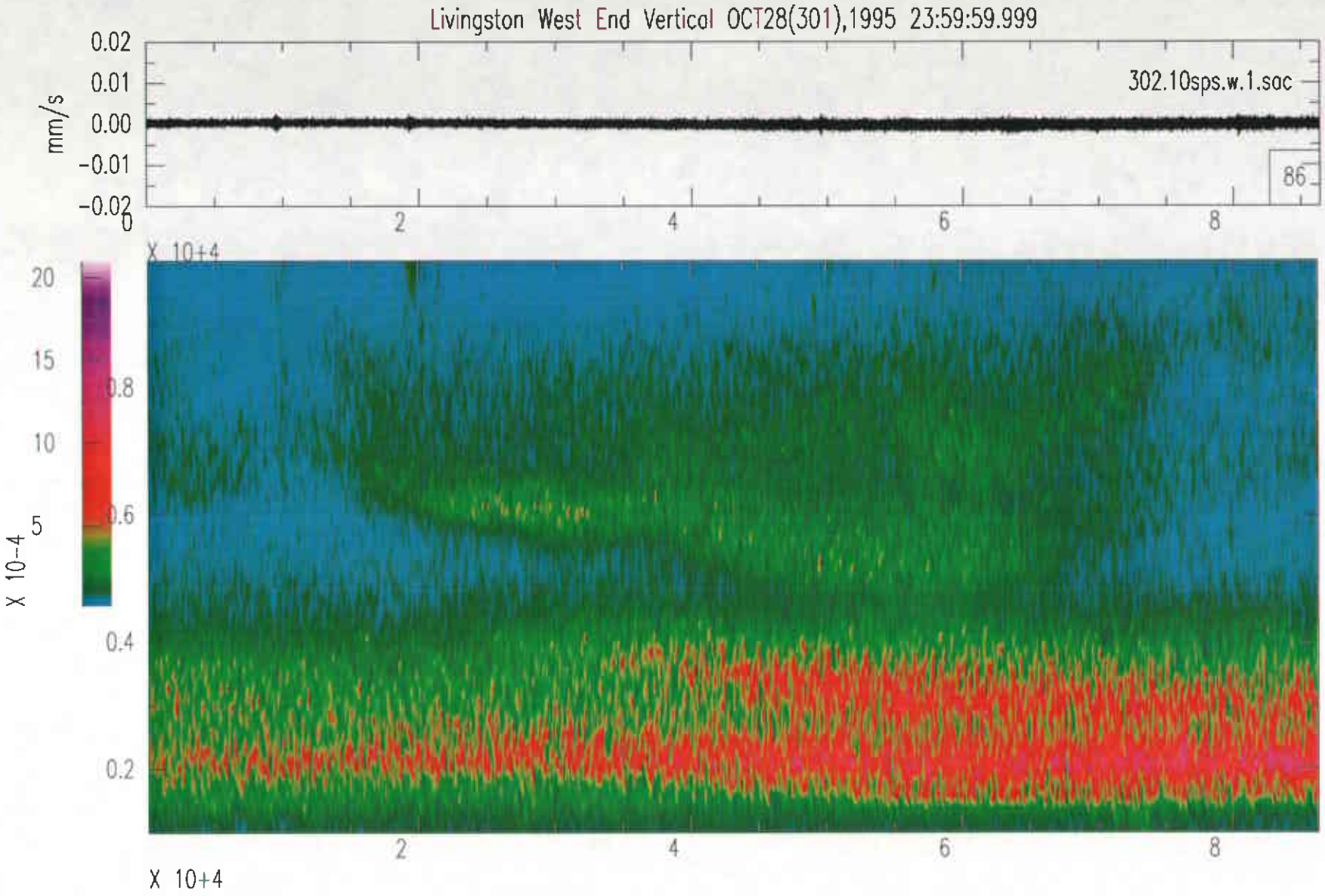
Livingston West End Vertical OCT28(301),1995 23:59:59.999
302.10sps.w.1.soc
86
mm/s
0.02
0.01
0.00
-0.01
-0.02
0
2
4
6
8
X 10+4
20
15
10
5
X 10-4
0.8
0.6
0.4
0.2
2
4
6
8
X 10+4

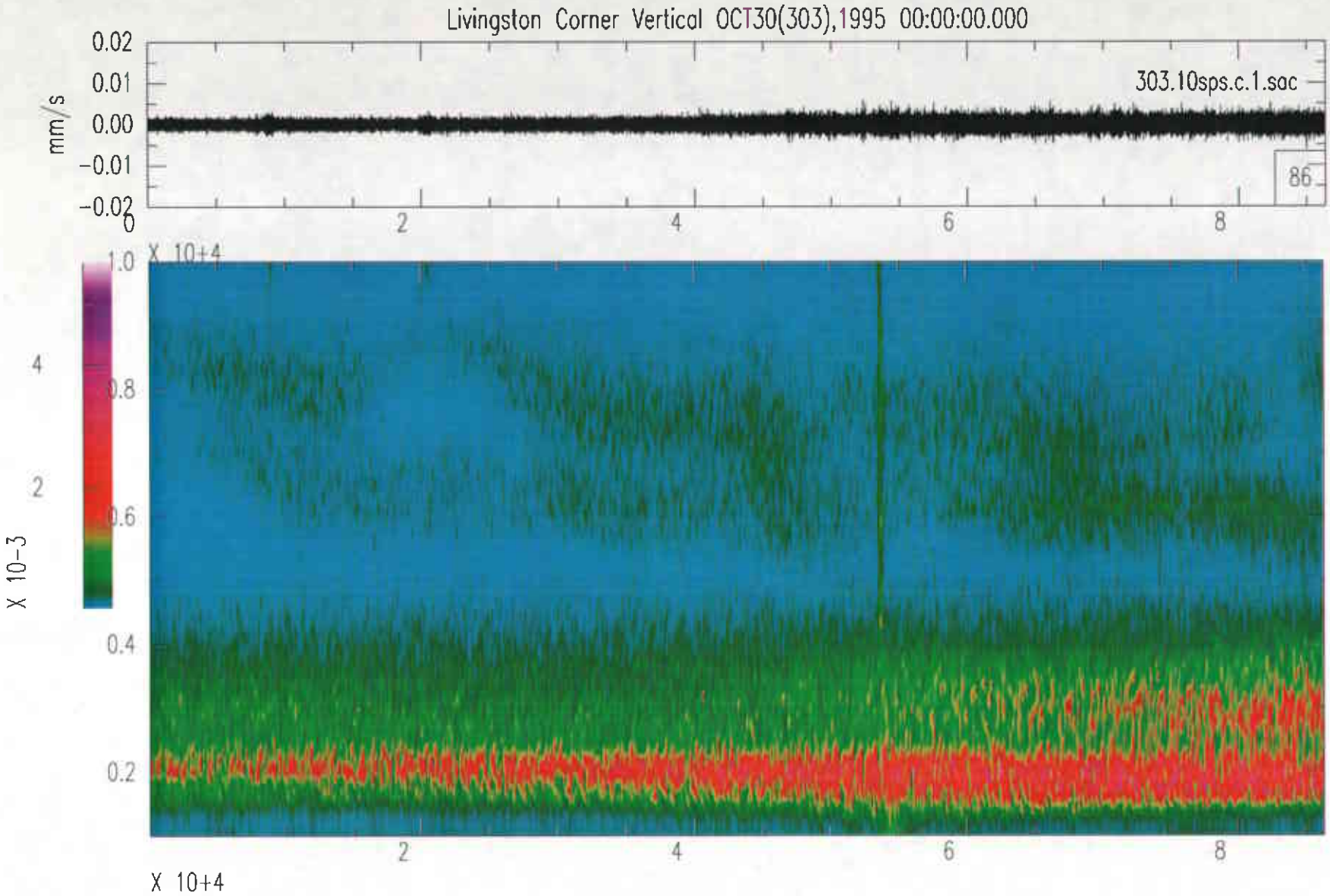
Livingston Corner Vertical OCT30(303),1995 00:00:00.000
303.10sps.c.1.sac
86
mm/s
0.02
0.01
0.00
-0.01
-0.02
0
2
4
6
8
X 10+4
1.0
0.8
0.6
0.4
0.2
X 10-3
4
2
X 10+4

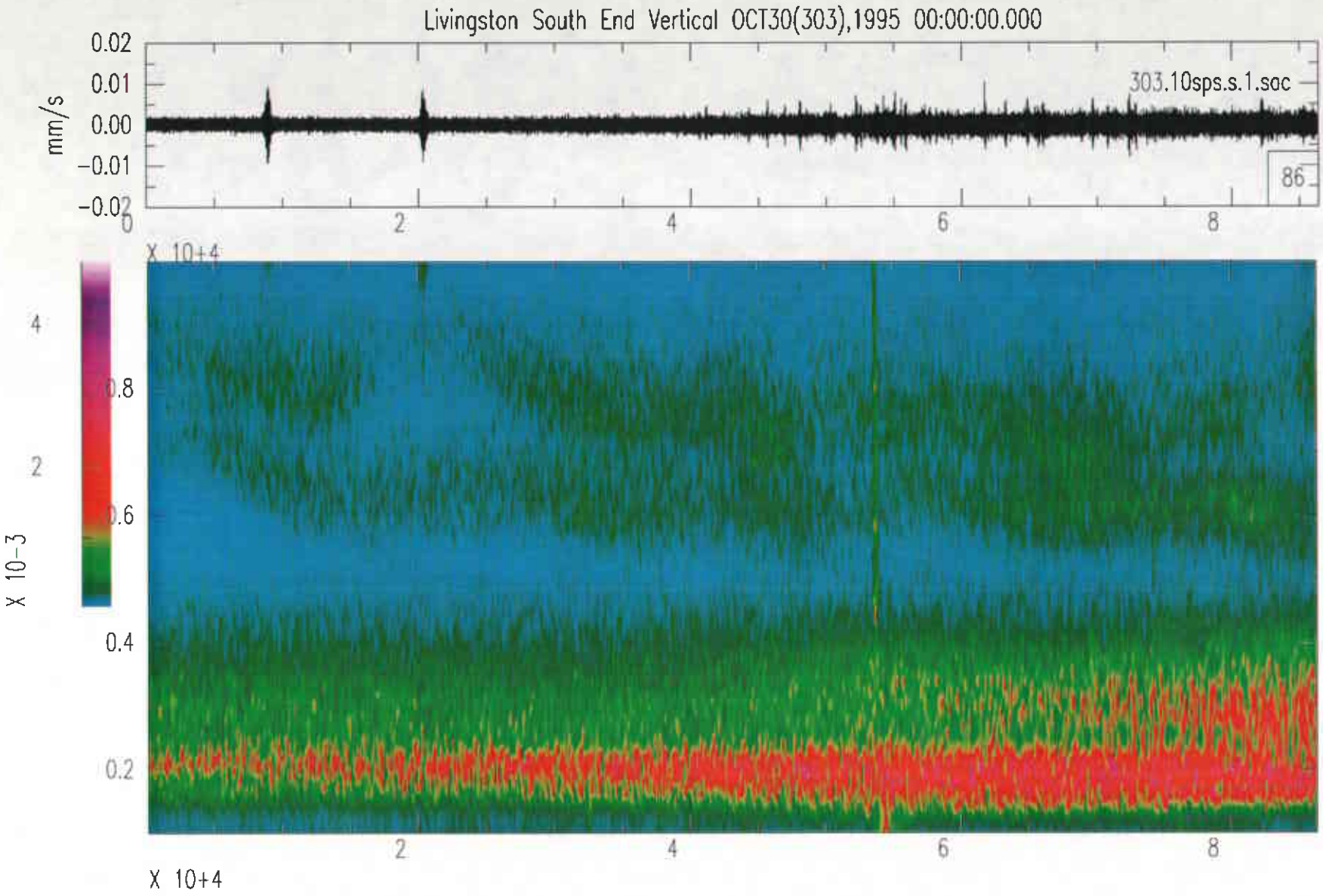
Livingston South End Vertical OCT30(303),1995 00:00:00.000
303.10sps.s.1.soc
86
mm/s
0.02
0.01
0.00
-0.01
-0.02
0
2
4
6
8
X 10+4
X 10-3
4
2
0.8
0.6
0.4
0.2
2
4
6
8
X 10+4

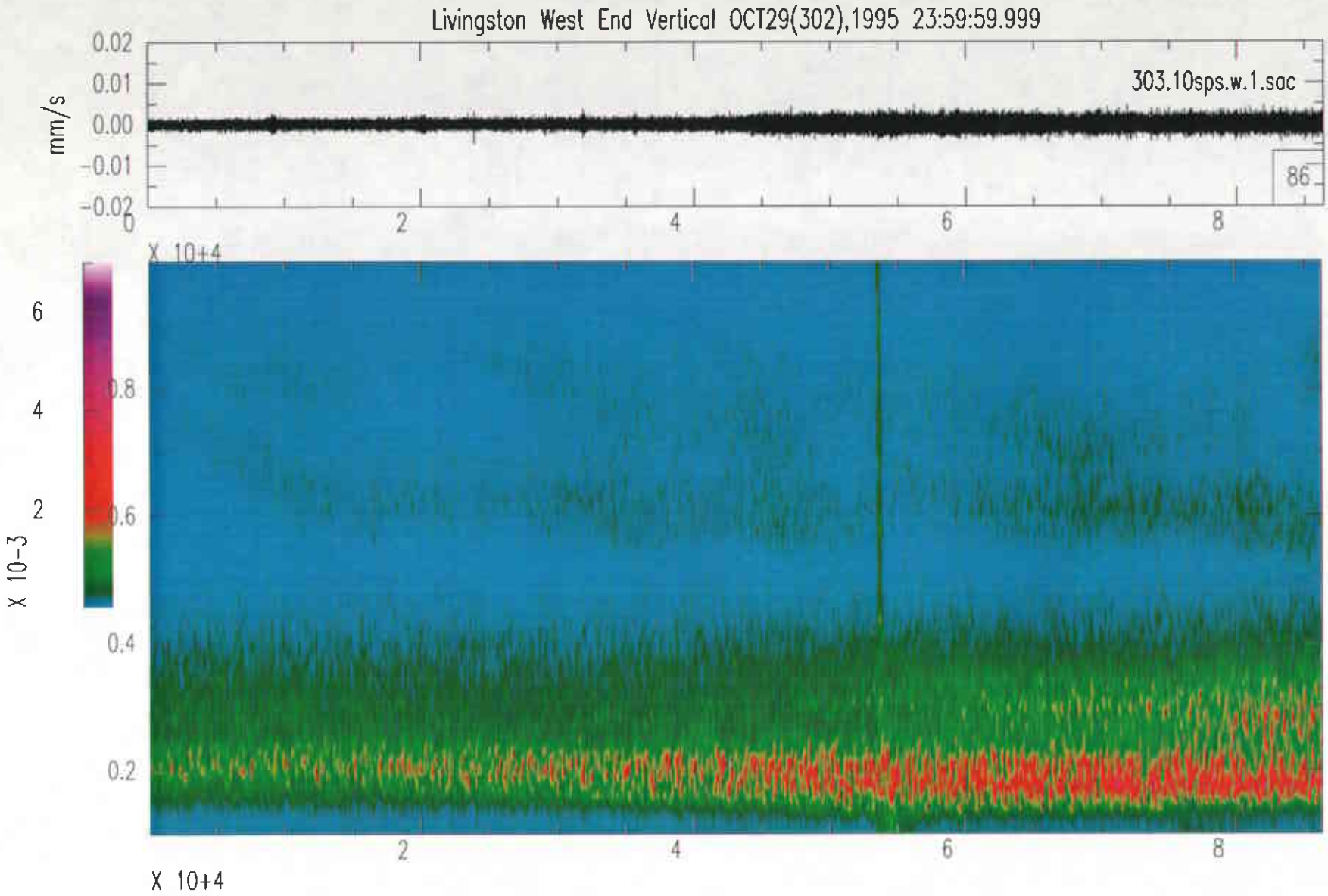
Livingston West End Vertical OCT29(302),1995 23:59:59.999
303.10sps.w.1.sac
86
mm/s
0.02
0.01
0.00
-0.01
-0.02
0
2
4
6
8
X 10+4
X 10-3
6
4
2
0.8
0.6
0.4
0.2
2
4
6
8
X 10+4

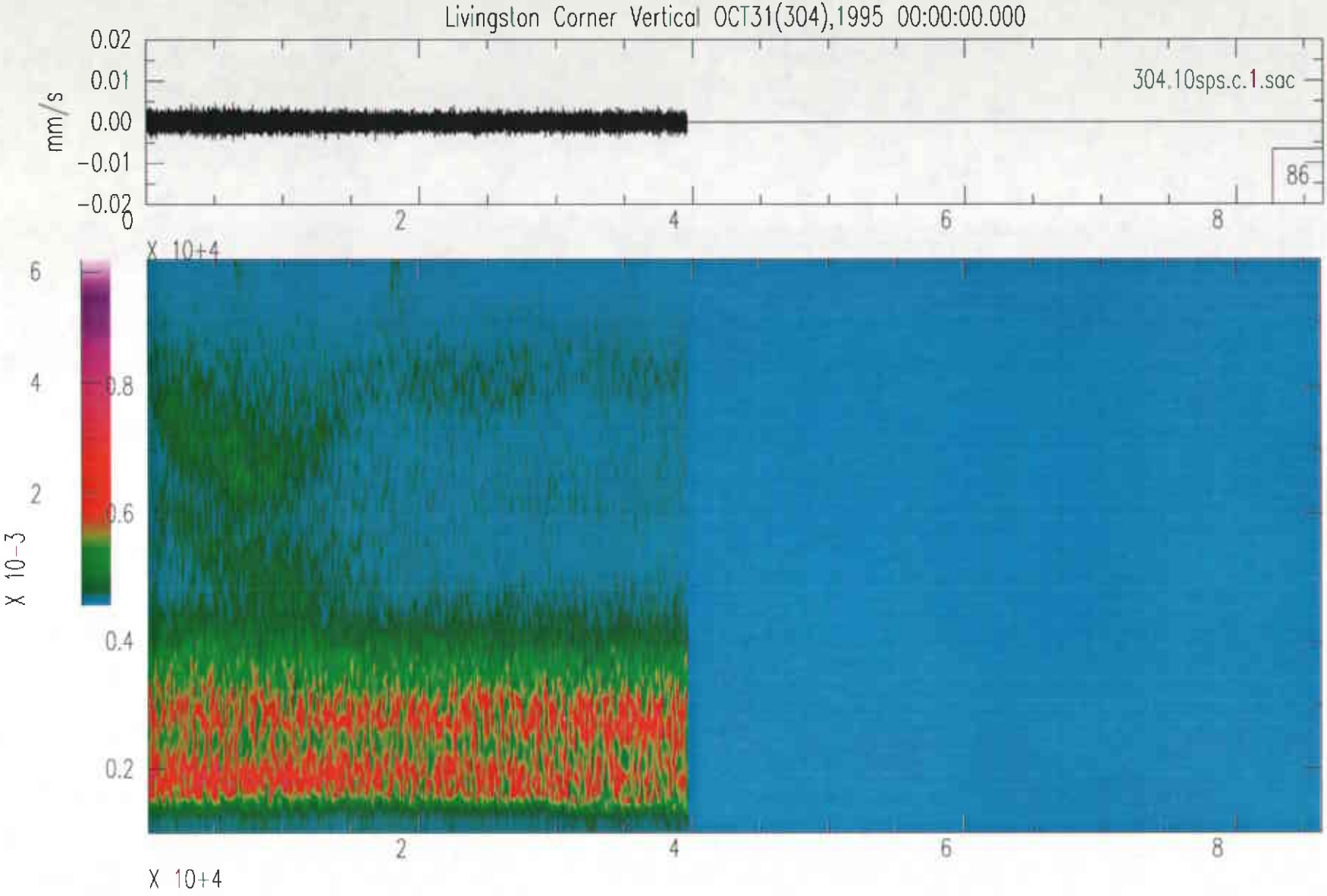
Livingston Corner Vertical OCT31(304),1995 00:00:00.000
304.10sps.c.1.sac
86
mm/s
0.02
0.01
0.00
-0.01
-0.02
0
2
4
6
8
X 10+4
X 10-3
0.8
0.6
0.4
0.2
X 10+4

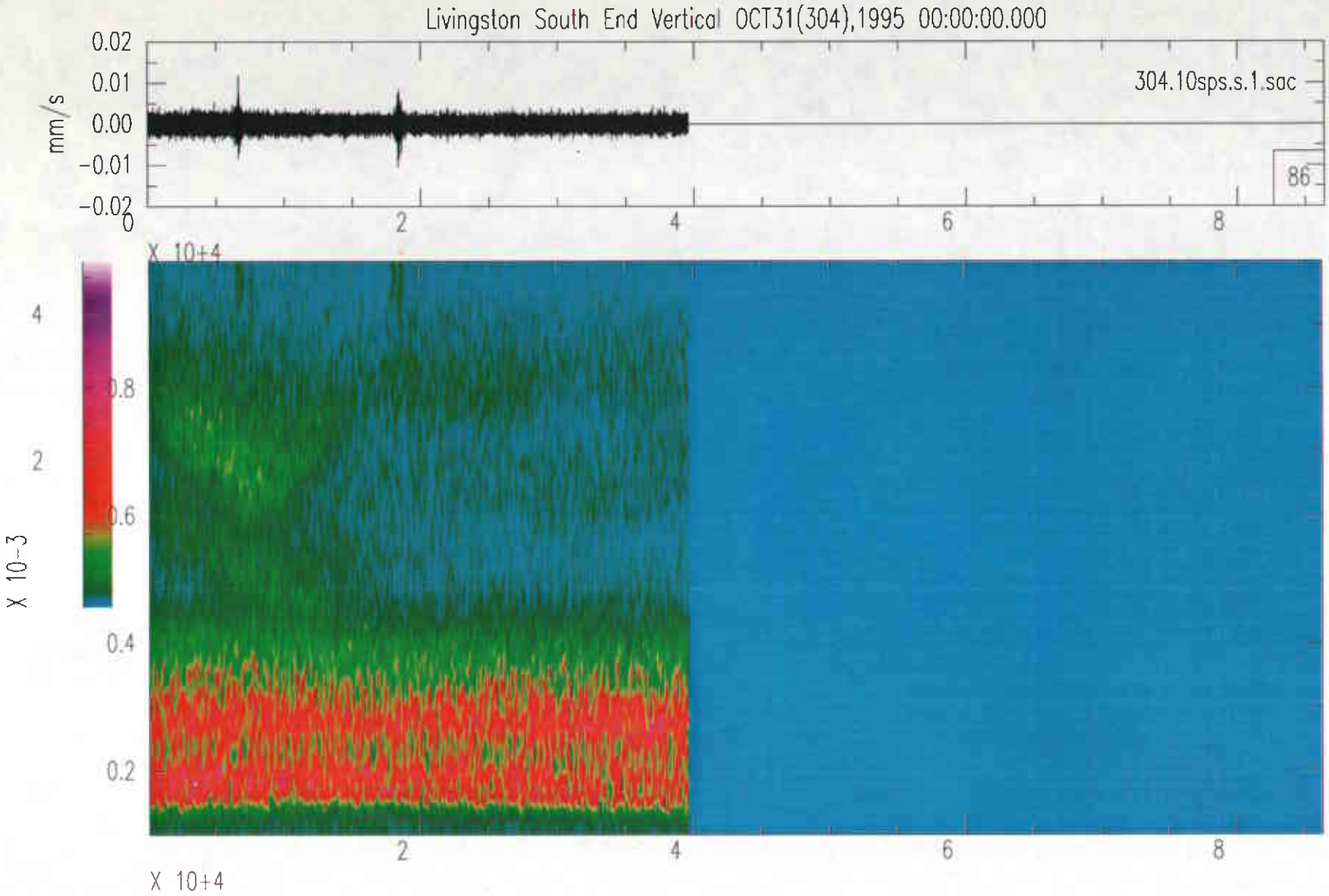
Livingston South End Vertical OCT31(304),1995 00:00:00.000
304.10sps.s.1.sac
86
mm/s
0.02
0.01
0.00
-0.01
-0.02
0
2
4
6
8
X 10+4
X 10-3
4
2
0.8
0.6
0.4
0.2
2
4
6
8
X 10+4

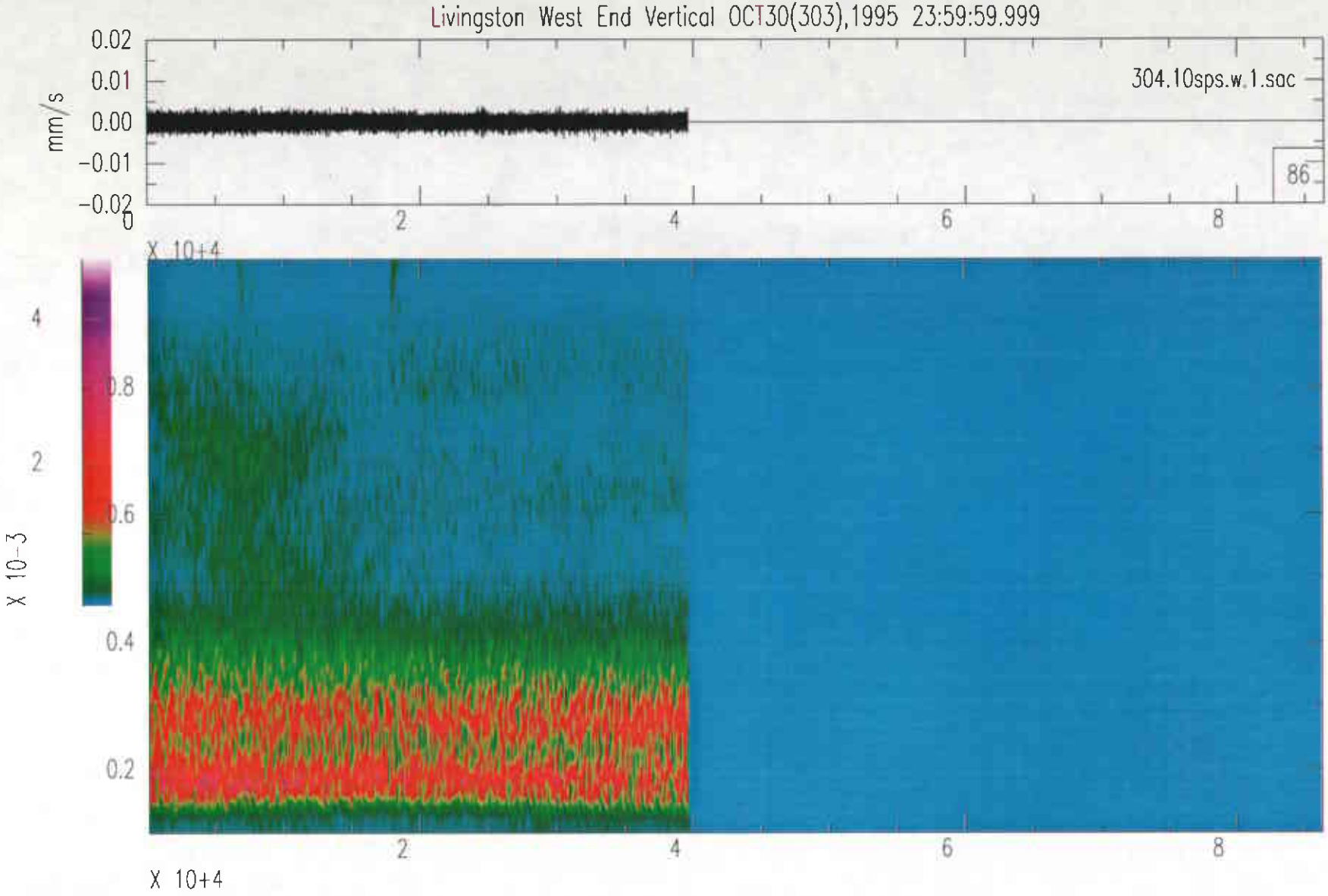
Livingston West End Vertical OCT30(303),1995 23:59:59.999
304.10sps.w.1.sac
86
mm/s
0.02
0.01
0.00
-0.01
-0.02
0
2
4
6
8
X 10+4
X 10-3
4
2
0.8
0.6
0.4
0.2
2
4
6
8
X 10+4

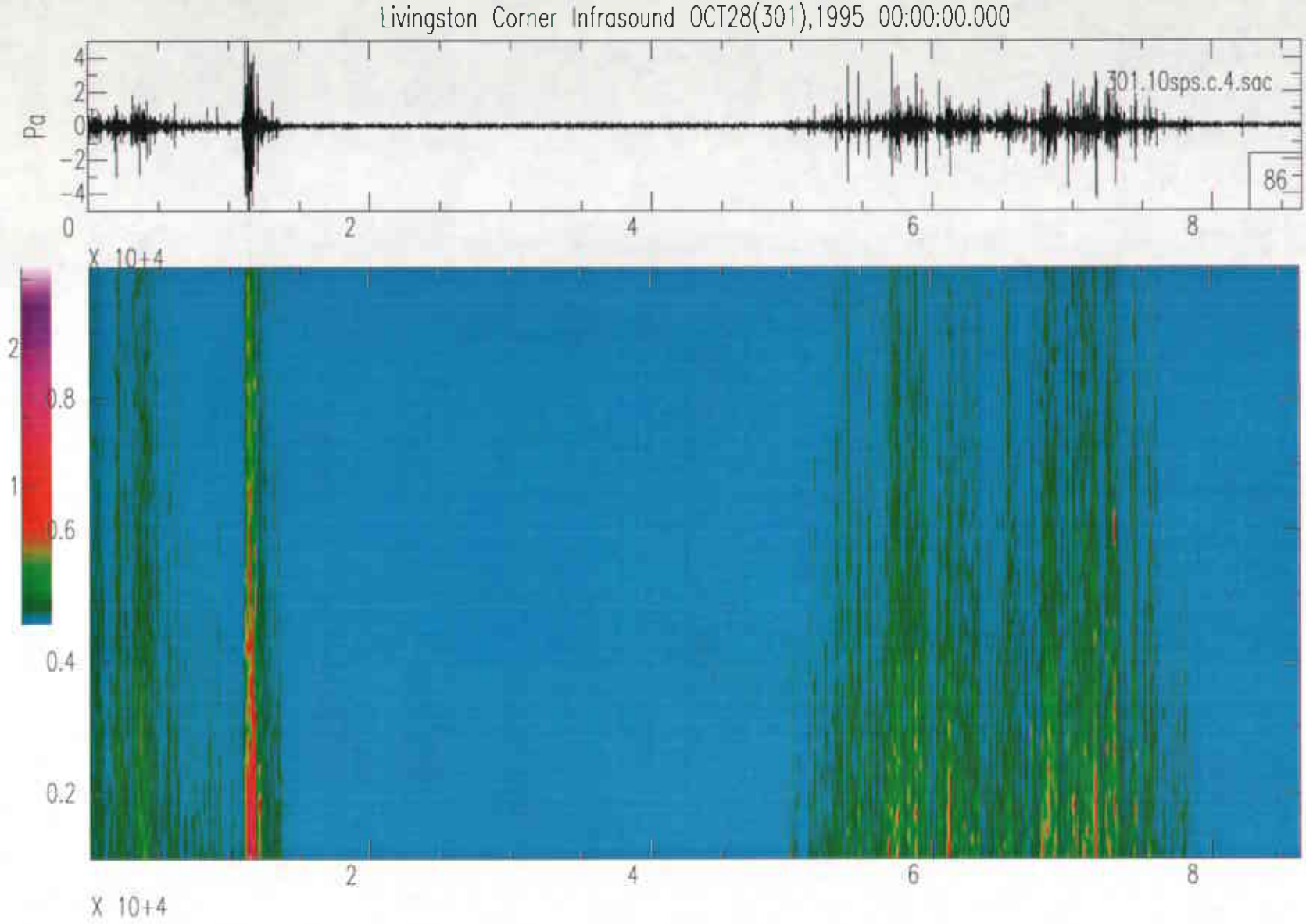
Livingston Corner Infrasound OCT28(301),1995 00:00:00.000
301.10sps.c.4.sac
86
Pa
4
2
0
-2
-4
0
2
4
6
8
X 10+4
2
1
0.8
0.6
0.4
0.2
2
4
6
8
X 10+4

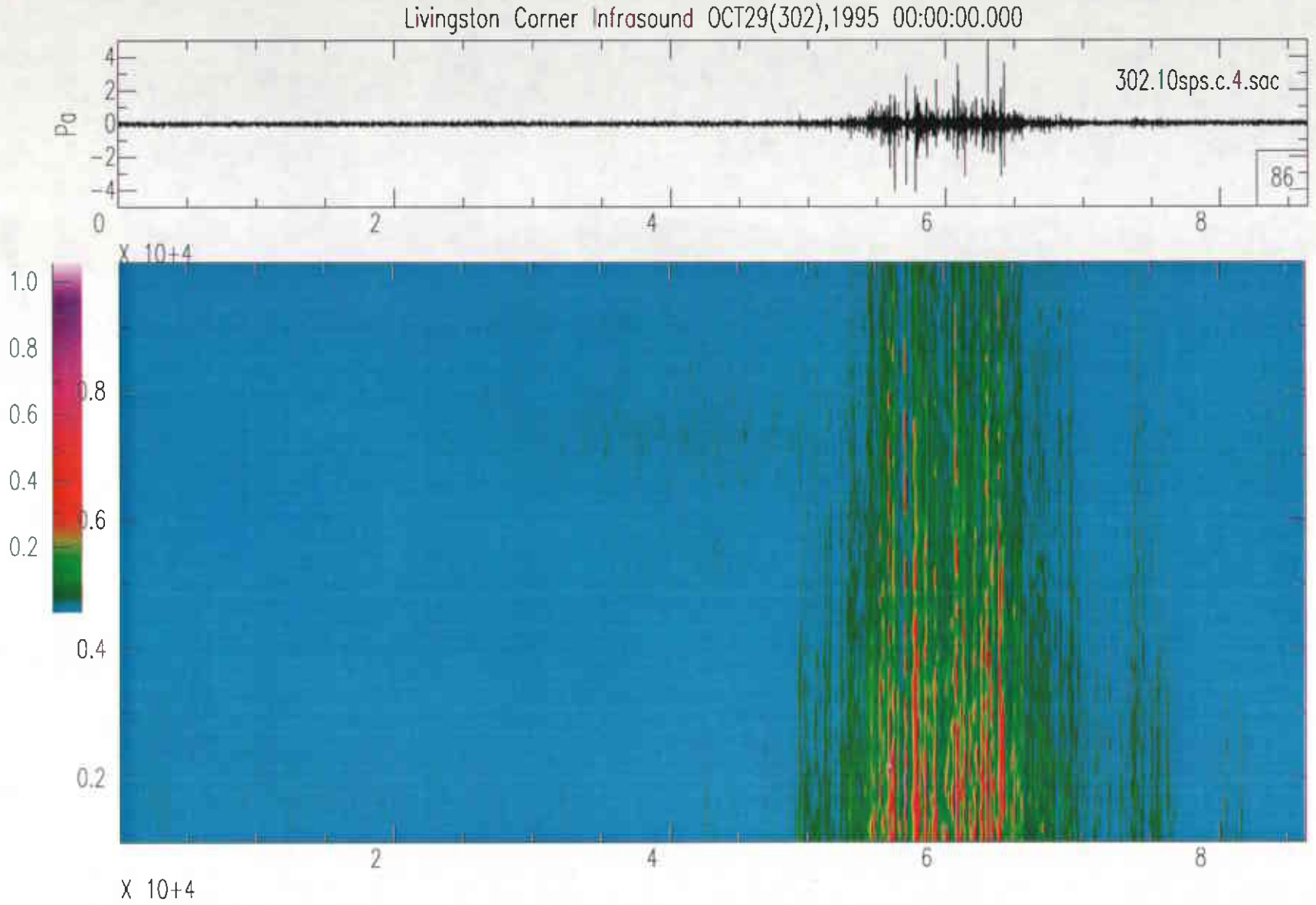
Livingston Corner Infrasound OCT29(302),1995 00:00:00.000
302.10sps.c.4.sac
Pa
86
X 10+4
X 10+4

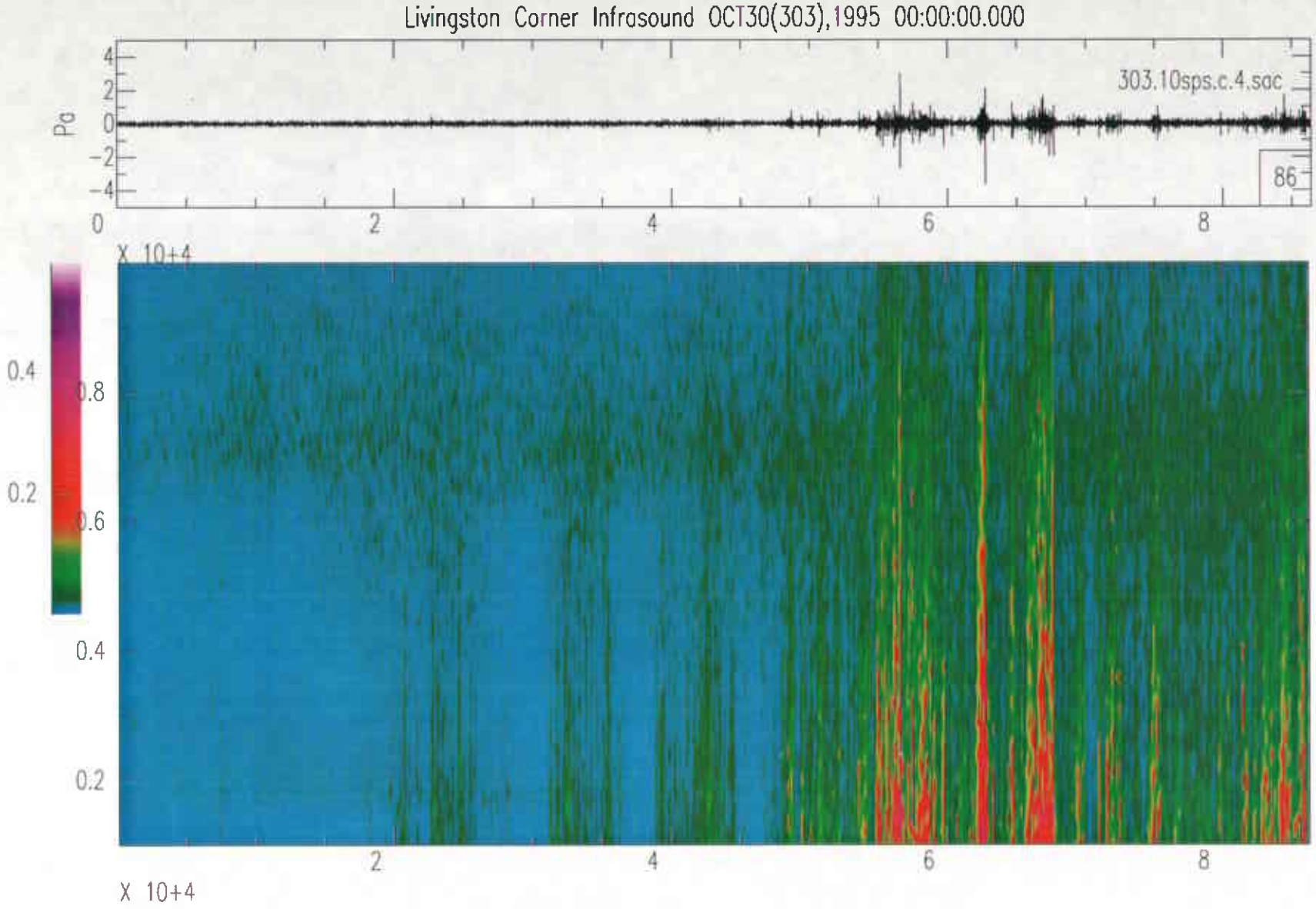
Livingston Corner Infrasound OCT30(303),1995 00:00:00.000
303.10sps.c.4.sac
Pa
4
2
0
-2
-4
86
0
2
4
6
8
X 10+4
0.4
0.8
0.2
0.6
0.4
0.2
2
4
6
8
X 10+4

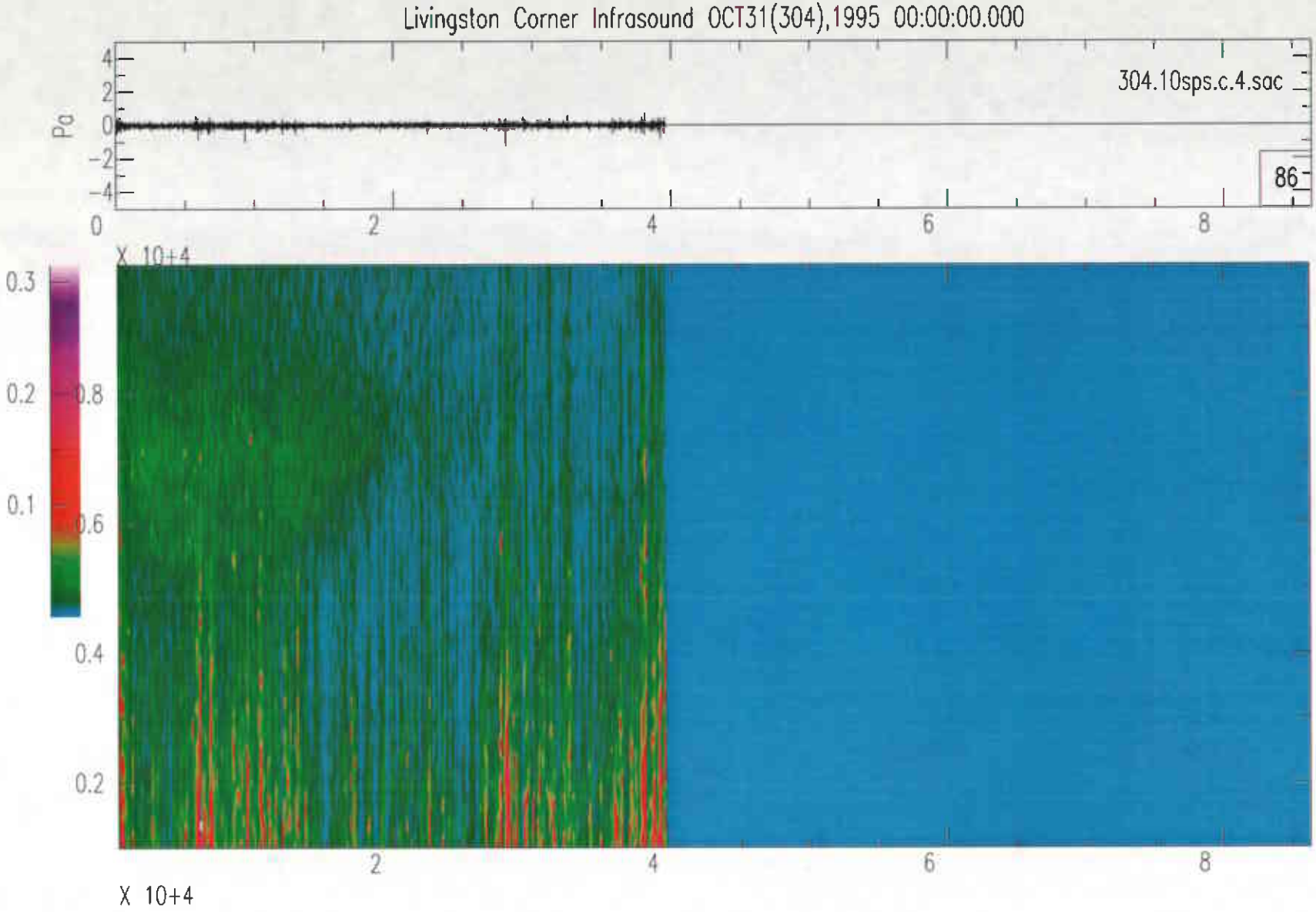
Livingston Corner Infrasound OCT31(304),1995 00:00:00.000
304.10sps.c.4.sac
Pa
86
X 10+4
0.3
0.2
0.1
0.8
0.6
0.4
0.2
X 10+4

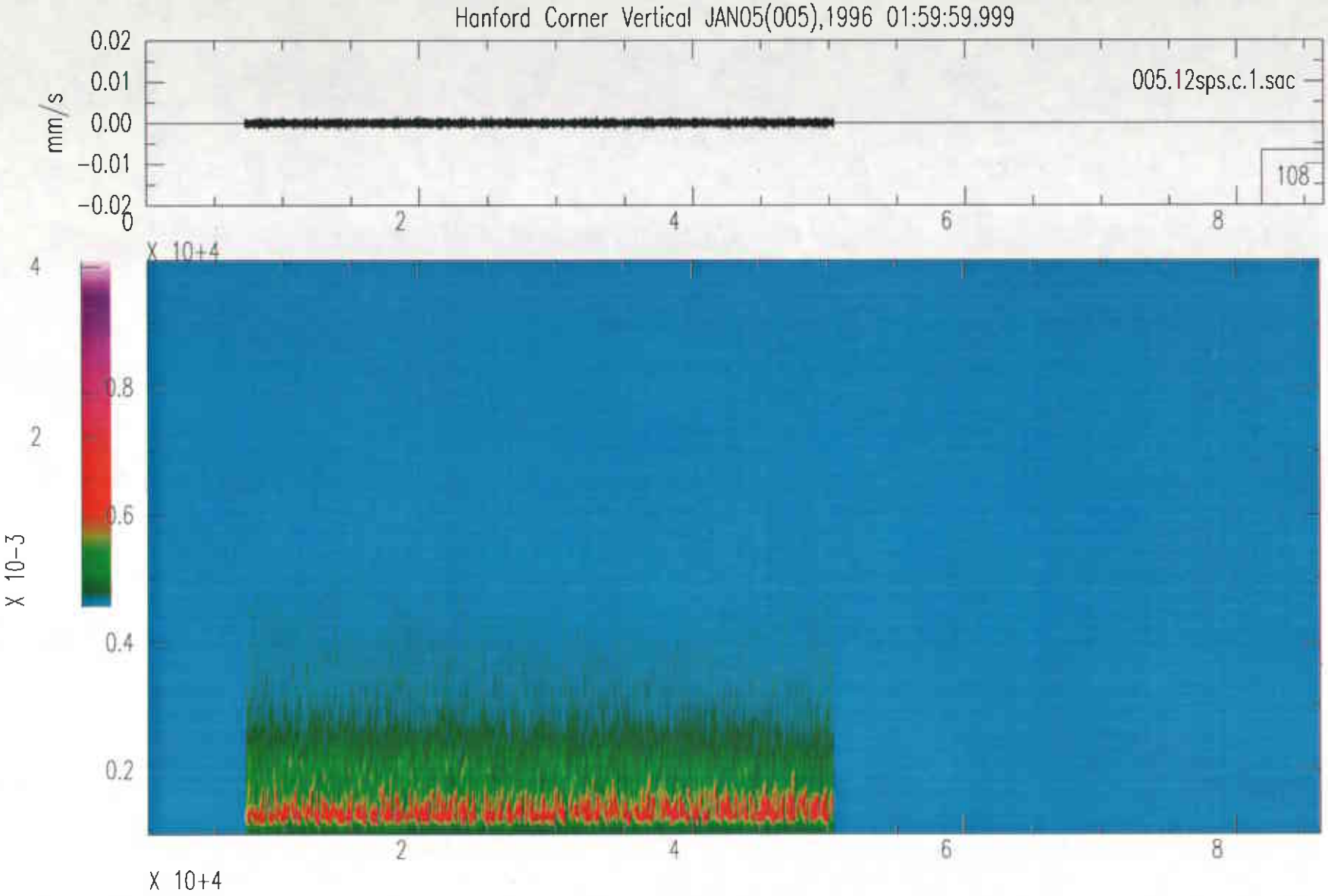
Hanford Corner Vertical JAN05(005),1996 01:59:59.999
005.12sps.c.1.sac
108
mm/s
0.02
0.01
0.00
-0.01
-0.02
0
2
4
6
8
X 10+4
X 10-3
4
2
0.8
0.6
0.4
0.2
X 10+4

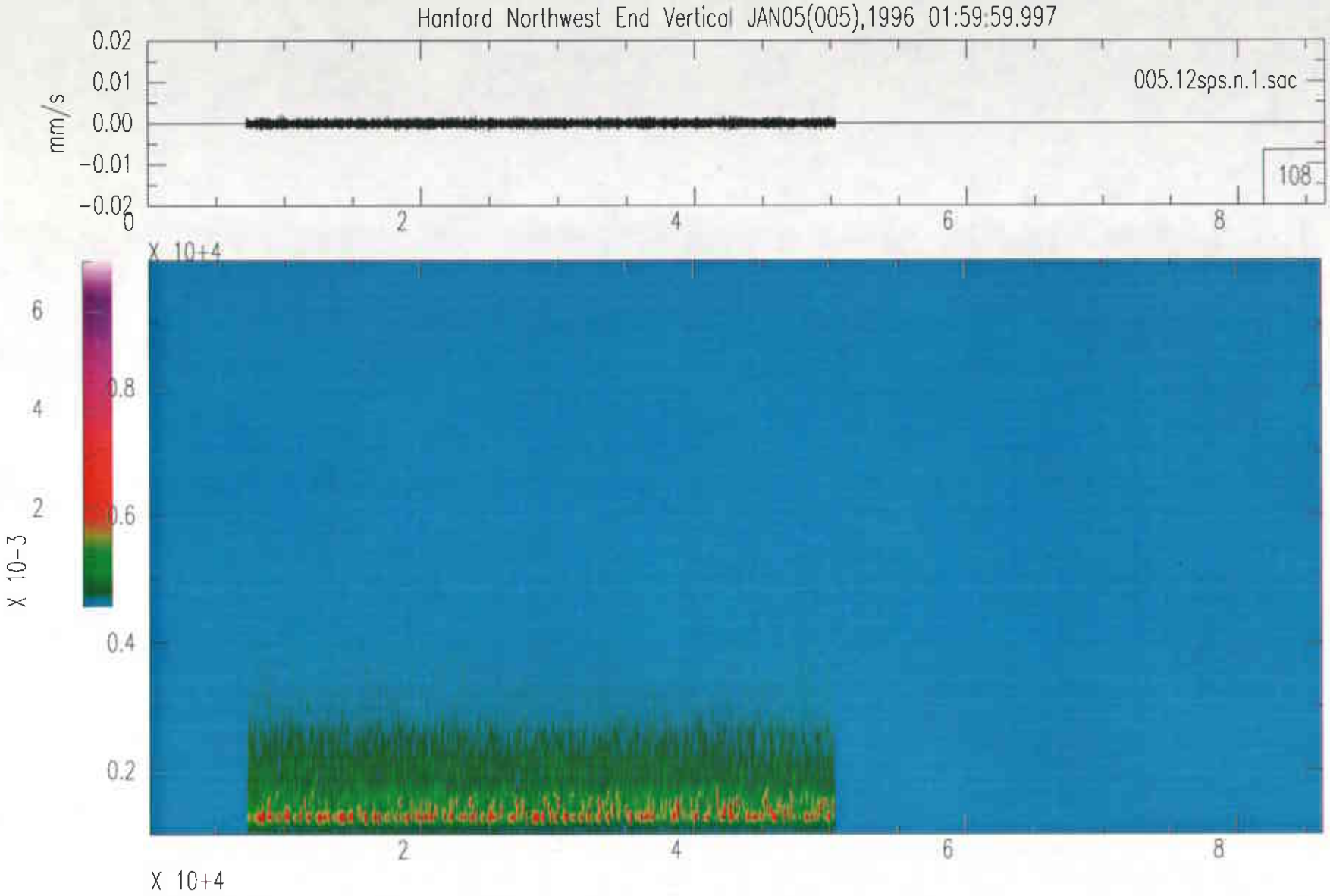
Hanford Northwest End Vertical JAN05(005),1996 01:59:59.997
005.12sps.n.1.sac
108
mm/s
0.02
0.01
0.00
-0.01
-0.02
0
2
4
6
8
X 10+4
X 10-3
6
4
2
0.8
0.6
0.4
0.2
2
4
6
8
X 10+4

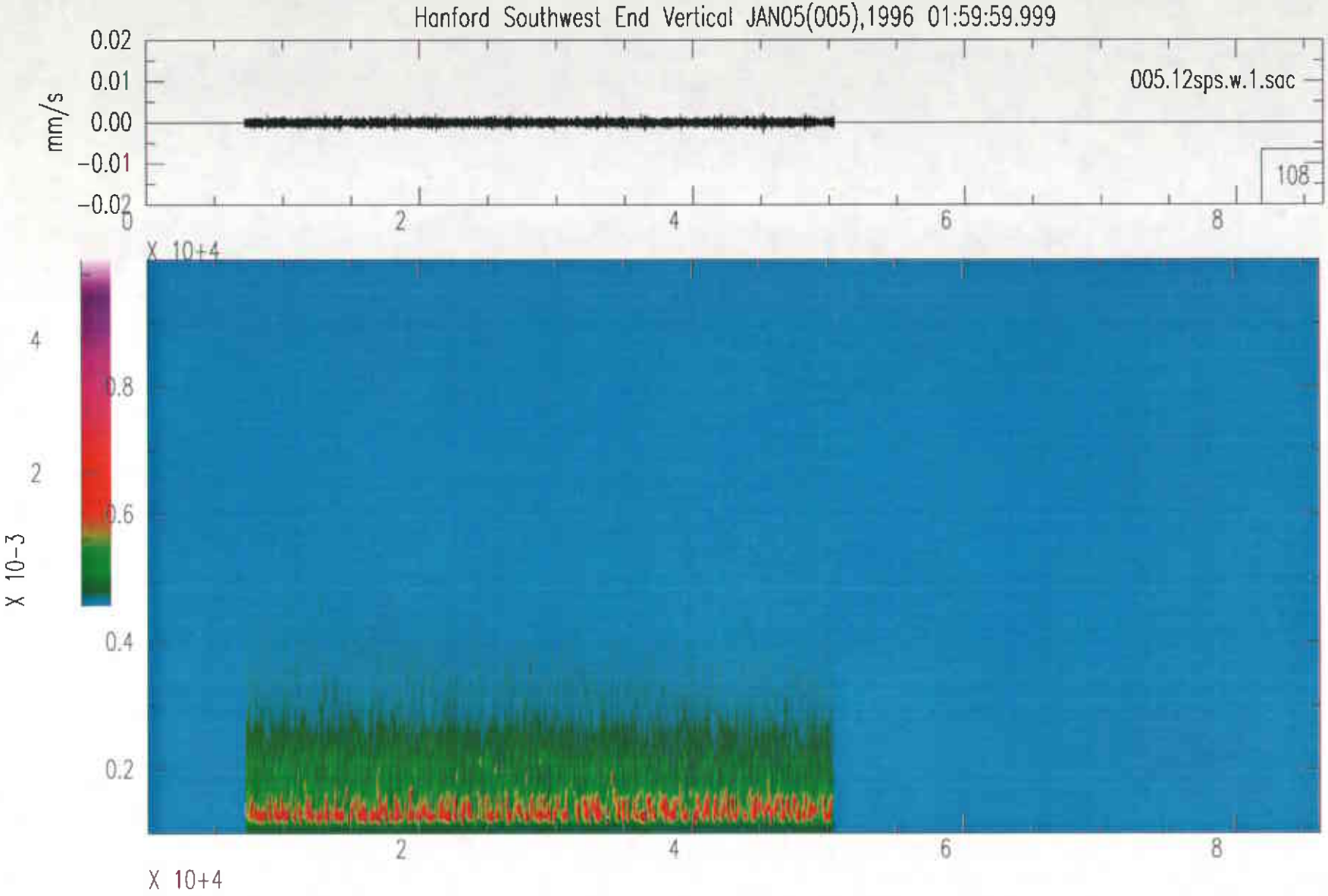
Hanford Southwest End Vertical JAN05(005),1996 01:59:59.999
mm/s
0.02
0.01
0.00
-0.01
-0.02
005.12sps.w.1.sac
108
0
2
4
6
8
X 10+4
X 10-3
4
2
0.8
0.6
0.4
0.2
2
4
6
8
X 10+4

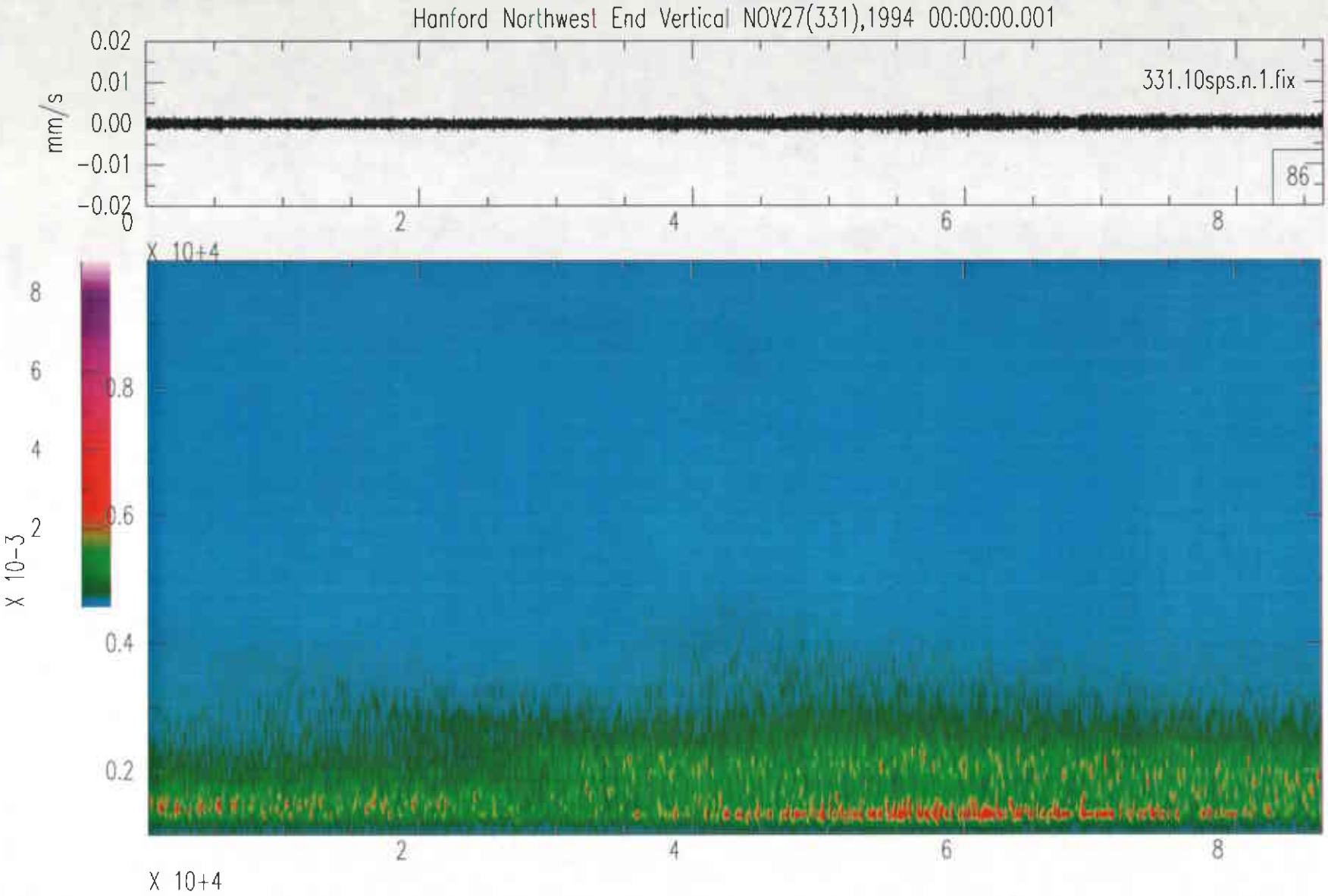
Hanford Northwest End Vertical NOV27(331),1994 00:00:00.001
331.10sps.n.1.fix
86
mm/s
0.02
0.01
0.00
-0.01
-0.02
0
2
4
6
8
X 10+4
X 10-3
8
6
4
2
0.8
0.6
0.4
0.2
2
4
6
8
X 10+4

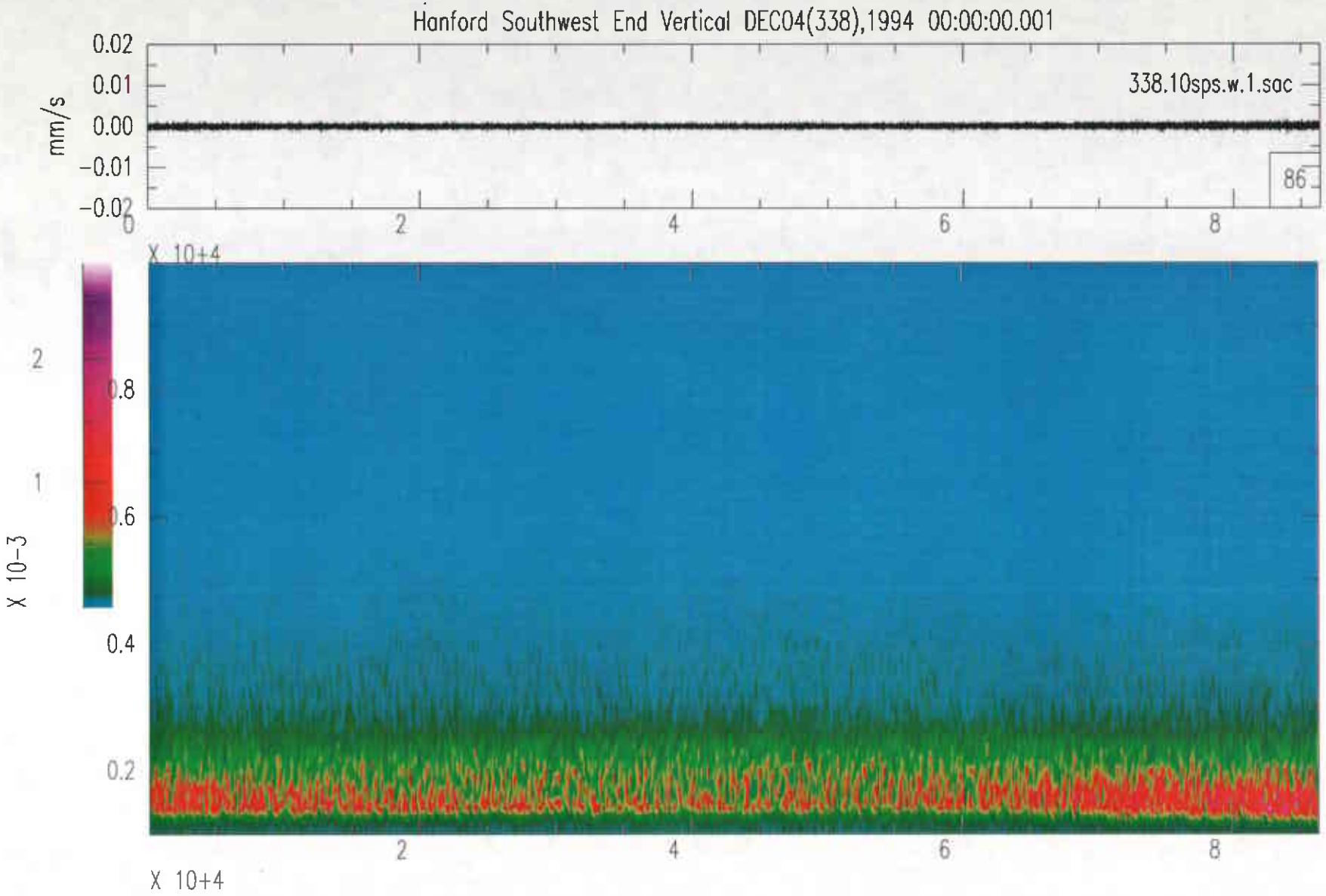
Hanford Southwest End Vertical DEC04(338),1994 00:00:00.001
0.02
0.01
0.00
-0.01
-0.02
mm/s
338.10sps.w.1.sac
86
0
2
4
6
8
X 10+4
2
1
X 10-3
0.8
0.6
0.4
0.2
2
4
6
8
X 10+4

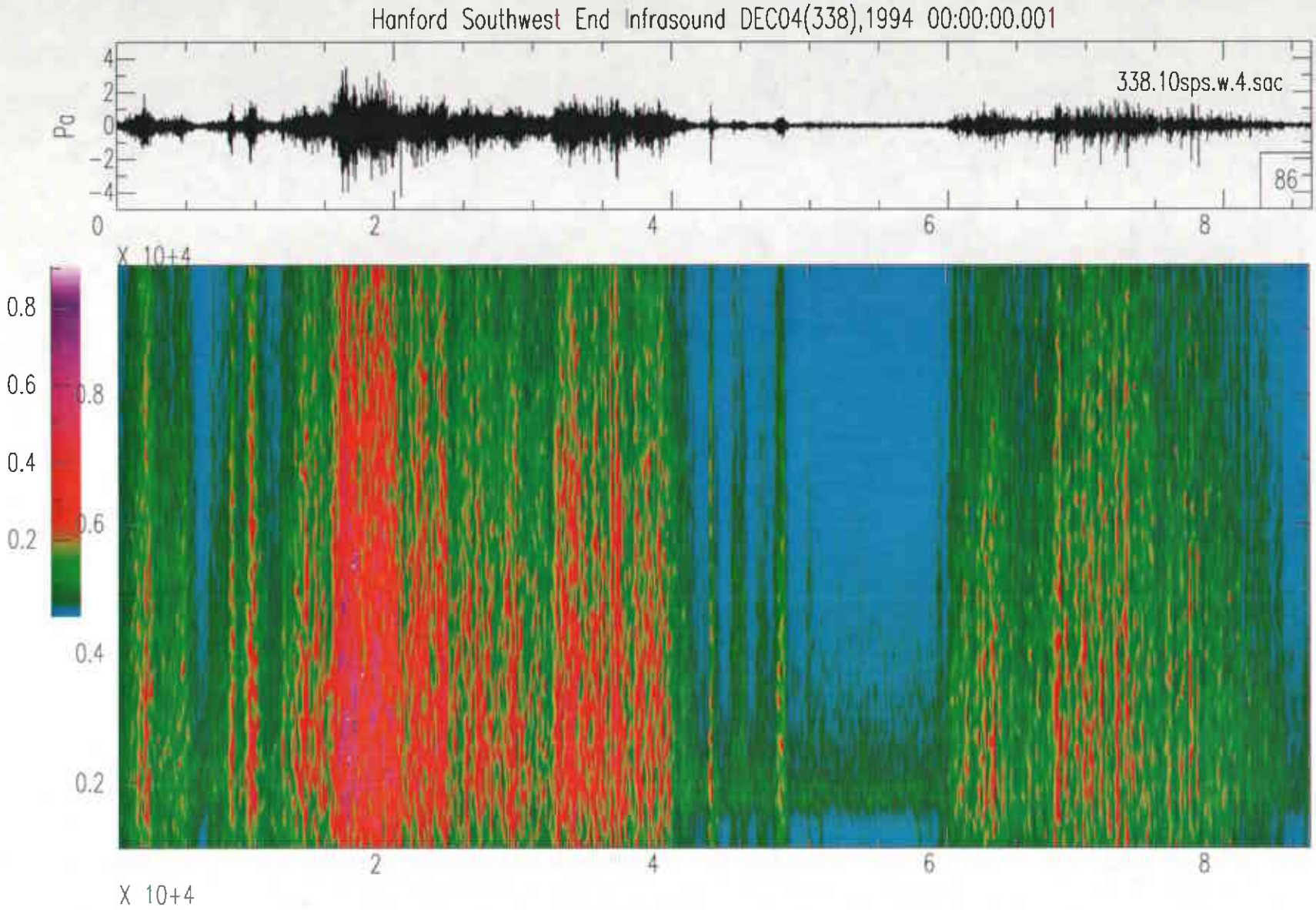
Hanford Southwest End Infrasound DEC04(338),1994 00:00:00.001
338.10sps.w.4.sac
Pa
4
2
0
-2
-4
86
0
2
4
6
8
X 10+4
0.8
0.6
0.4
0.2
0.8
0.6
0.4
0.2
2
4
6
8
X 10+4

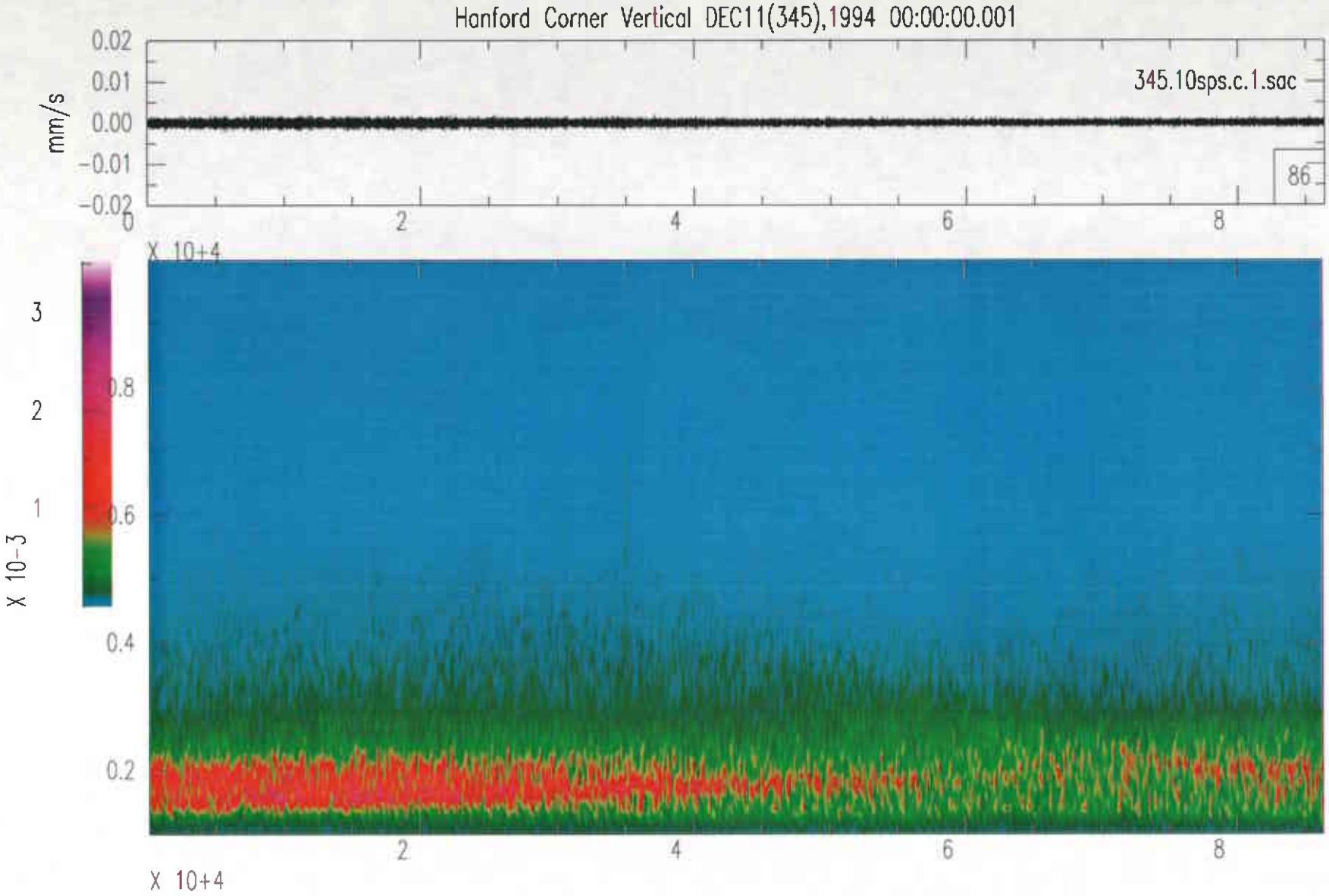
Hanford Corner Vertical DEC11(345),1994 00:00:00.001
345.10sps.c.1.sac
86
mm/s
0.02
0.01
0.00
-0.01
-0.02
0
2
4
6
8
X 10+4
X 10-3
3
2
1
0.8
0.6
0.4
0.2
2
4
6
8
X 10+4

Appendix B

Wavenumber Analysis

Introduction. A wavenumber analysis conducted on the low-frequency signals at the LIGO sites at Hanford and Livingston indicates substantial differences in the structure of the noise wave field. At the Hanford site, fast-propagating waves are observed with velocities near 3.5 km/s, consistent with Rayleigh wave propagation in the region, but there are many periods when higher velocities are observed that are more typical of body waves. Sources from westerly directions are frequently observed, as expected from sources in the Pacific Ocean or near the Pacific Coast, but noise travelling from northeastern directions is observed just as frequently.

At Livingston, wave propagation velocities are concentrated at slower velocities near 2 km/s, and the dominant direction of approach is north-northeast. The geography of the Livingston LIGO area suggests that the microseism noise might be generated from sources in the Gulf of Mexico, although sources in the more distant Atlantic Ocean are also expected. Wind-generated waves in Lake Pontchartrain could also generate a "lake-effect" that might be observed at Livingston. There may be significant differences in how microseism waves are generated and propagated from these potential sources because of the differences in the areas and depths of the water bodies, and in the characteristics of shorelines bordering them. The geologic structure is known to be dominated by a thick sedimentary sequence at shallow depths implying low seismic velocities in the uppermost 5 km, but the velocity structure is very poorly known at greater depth.

At Hanford, particular wave shapes observed in the time series can be tracked from location to location, but this is not the case at Livingston, where wave shapes have different appearances. This may be indicative of an interference pattern from sets of waves crossing the array from different directions and at different velocities, but this cannot be resolved with just the tripartite array formed by the three measurement locations. The dissimilar wave shapes, combined with large phase differences (approaching 180 degrees) make interpretation of the wavenumber results ambiguous at Livingston. To insure that the data were properly taken and analyzed at Livingston, the following analysis of a series of fast-moving waves from a distant earthquake is presented, which provides an introduction to the wavenumber method used.

Analysis of earthquake signal correlation. The timing and response of the three measurement installations at Livingston can be demonstrated to be empirically correct by analyzing the signals from a distant earthquake. The earthquake had a magnitude of 6.4 and was located near the coast of central Chile (28.9 S, 71.4 W) on Day 305 at 00:35:32 GMT. Positive polarity compressional waves are expected at Livingston, and a standard earth velocity model predicts an apparent velocity of 16 km/s (the waves arrive from a near vertical inclination) from an azimuth of 161 degrees. This practically coincides with the orientation of the South Arm of the LIGO facility, so it implies that the South End should detect these waves in advance of the Corner by 0.25 s, and the West End should detect these waves simultaneously with the Corner.

Figure B-1 shows the time series from all three vertical-component channels (the bottom plot shows the corrected response of the 30-s seismometer). This plot clearly illustrates the coherence of the earthquake signals. (It also shows an example of the lack of coherence of the noise preceding the arrival of the earthquake signals.) Other sections of the earthquake signal were also examined for the three north-south and three east-west channels to insure that all signals had the correct polarity and amplitude.

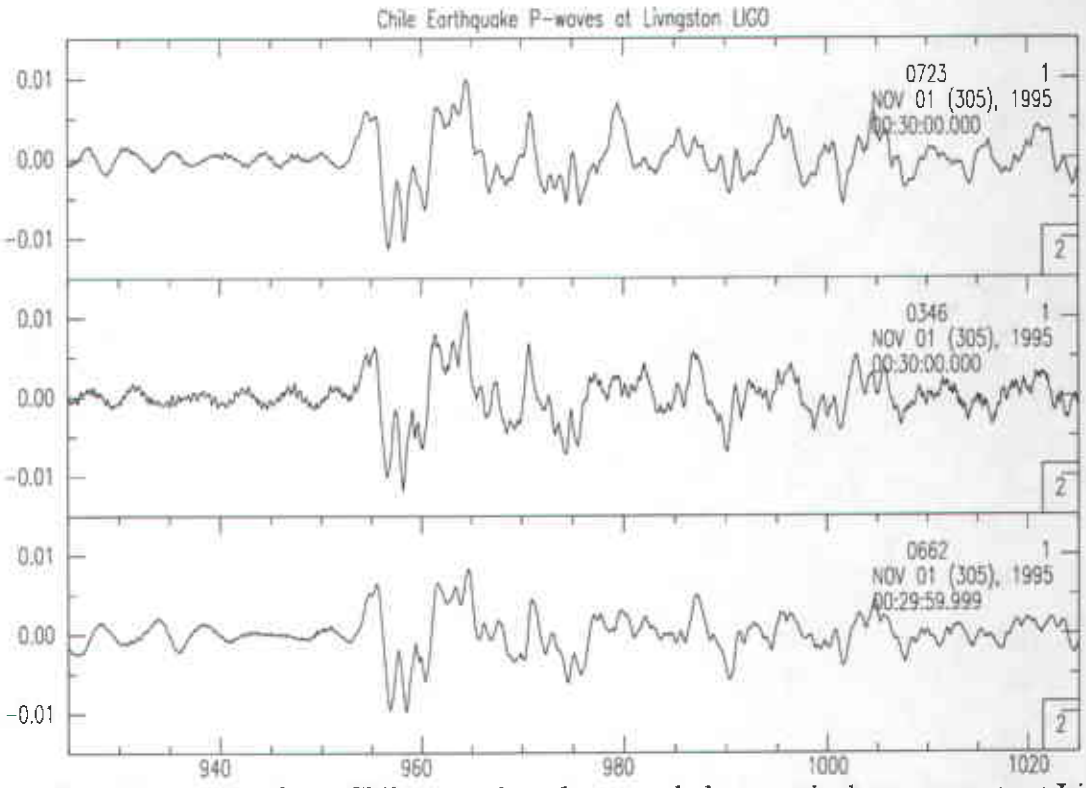

Figure B-1. Time series from Chilean earthquake recorded on vertical components at Livingston LIGO site.

The wavenumber analysis attempts to determine the vector velocity of a plane wave crossing the array formed by the three sensors. The analysis projects the power of the combined three signals onto the two-dimensional wavenumber plane. The peak power on the wavenumber plane is then selected to represent an azimuth of approach and a propagation velocity. A segment of the three vertical signals was taken and the ends of the segment were tapered to zero to remove end effects for the subsequent two-pass (forward and reversed) band-pass filtering.

Wavenumber analyses for two filter bands, from 0.1 to 0.2 Hz and from 0.8 to 1.0 Hz, are shown in Figure B-2, where the combined power of the three signals is contoured as a function of the two horizontal wavenumbers. The peak amplitude occurs at 0.008 and 0.035 cycles/km. The propagation velocity is determined by the ratio of the peak frequency f (in cycles/s or Hz) and the wavenumber k (in cycles/km) using v = f/k. The velocity determined for the two analyses is 19-25 km/s, for comparison to that predicted, 16 km/s. The azimuth estimated from the wavenumber diagrams is from an eastern or southeastern direction, compared to the predicted southeastern azimuth of 161 degrees.

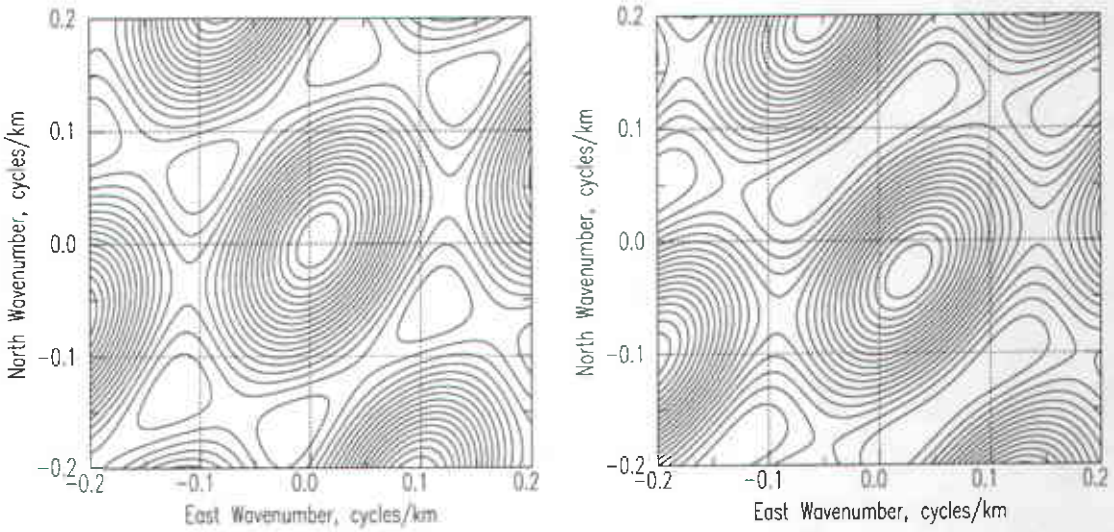

Figure B-2. Wavenumber results from compressional-wave time window for Chilean earthquake.The contour plots show the combined power of the three vertical-component signals contoured as a function of wavenumber in the two horizontal directions. Left contour plot is for earthquake signals band-passed from 100-200 mHz. Right contour plot is for 800-1000 mHz.

Direct measurements of time delays between earthquake signals from signal cross-correlation indicate that the South End was advanced relative to the Corner by only 0.16 s, but that the West End was also delayed by 0.12 s relative to the Corner. This implies a travel time over a 4 km distance equal to the geometrical sum of the delays (sqrt(0.16^2 + 0.12^2)) or a 4-km travel time of 0.2 s. Using simple geometry, the result is that the signals are crossing the array at 20 km/s from an azimuth of 125 degrees, in approximate agreement with the higher-frequency wavenumber result. Similar results were obtained using other portions of the earthquake signal as recorded on the horizontal components.

It is common for earthquake travel times to be systematically delayed or advanced by 0.1 s at different locations, but there are no significant elevation differences between the three measurement locations, nor any significant seismic velocity differences expected beneath these locations. This suggests that there are physical and/or numerical limits to the noise correlation results within a resolution of 0.1 s, but this is a relatively small portion of the period and expected transit time of observed microseisms.

Wavenumber analysis of peak microseism noise. The amplitude spectra at Hanford and Livingston indicate that the microseism peak occurs at different frequencies at the two sites. At Hanford, a sharp peak is consistently near 0.125 Hz (8 second period). At Livingston, a broader peak is observed between 0.15 and 0.2 Hz (5-7 second period). The wavenumber analysis focuses on a narrow frequency band at the peak frequency at each of the two sites. Frequency bands of 100-150 mHz and 150-200 mHz were appropriate for a comparative analysis of the maximum noise peak at Hanford and Livingston, respectively. The analysis was conducted using both frequency bands at each site for comparison. Only the vertical channel has been analyzed, because the amplitude changes with wave direc-

tion when a preferred horizontal polarization exists (as is expected for Rayleigh wave propagation). Filtering in these two bands was done with a 2-pole Butterworth filter operated on both the forward and reversed time series to eliminate the filters' phase shifts. Filtering was conducted on one-hour data segments with the first and last 0.5% (18 seconds) tapered to zero to eliminate filter transients.

The one-hour filtered data were then windowed into overlapping 60-s segments using a squared, raised cosine bell to strongly enhance the middle 30 s of the data. This obtains 4-5 cycles of the noise for each wavenumber measurement. The window was shifted 30 s for each subsequent measurement. The windowed time series amplitudes were normalized so that the peak amplitude output of the wavenumber analysis at Hanford was approximately unity for the 100-150 mHz band.

The wavenumber analysis selects the peak power on the two-dimensional wavenumber plane to represent the azimuth of approach and propagation velocity. The search for the peak power was restricted to a wavenumber k (in cycles/km) less than the highest frequency f (in cycles/s or Hz) of the filter pass band. The slowest velocity allowed is thus 1 km/s, given the rule f/k >1 km/s. The restriction to propagation velocities greater than 1 km/s is partially based upon the expected propagation velocity, but there can remain ambiguity in the determination of the direction and propagation velocity within this limit.

Figure B-3 shows two examples of wavenumber analyses at Hanford. The example on the left shows a time segment when all three signals were practically identical in phase, resulting in the central peak at zero (infinite apparent velocity that corresponds to vertically-propagated body waves). The example on the right shows the opposite extreme, where two peaks are observed with nearly equal wavenumbers having azimuths separated 180 degrees from each other. The ambient noise at the Southwest End and Corner during this time segment are out of phase by 180 degrees, and the Northwest End and Corner are nearly in phase. The wavenumbers for either peak are near 0.125 cycles/km, and from the frequency of 125 mHz, a propagation velocity of 1 km/s along either direction of the Southwest Arm results (which is much slower than expected for Rayleigh waves). This situation simply corresponds to a time delay/advance of 4 s, half of the 8-s period.

At Livingston, where the frequency is higher, near 185 mHz, it is more difficult to select a unique maximum on the wavenumber plane. Figure B-4 shows two examples of the wavenumber analyses there. The contour diagram on the right has a unique (closest to zero) peak on the wavenumber plane, and choosing this as the correct value, a velocity near 2 km/s is determined (the wavenumber near 0.09 cycles/km). This example (the right side of Figure B-4) is the typical result at the Livingston site. The phase at both Ends is delayed equally by 1.4 s relative to the Corner in this example.

The example on the left side of Figure B-4 shows a similar example, but in this case, there can be alternative choices within the limitation f/k>1. The two maxima have wavenumbers near 0.14 cycles/km and so a velocity of approximately 1.3 km/s results, either in a northerly or a southeastern direction. If even slower velocities are possible, then the two maxima on the left half of the wavenumber plane could also be considered.

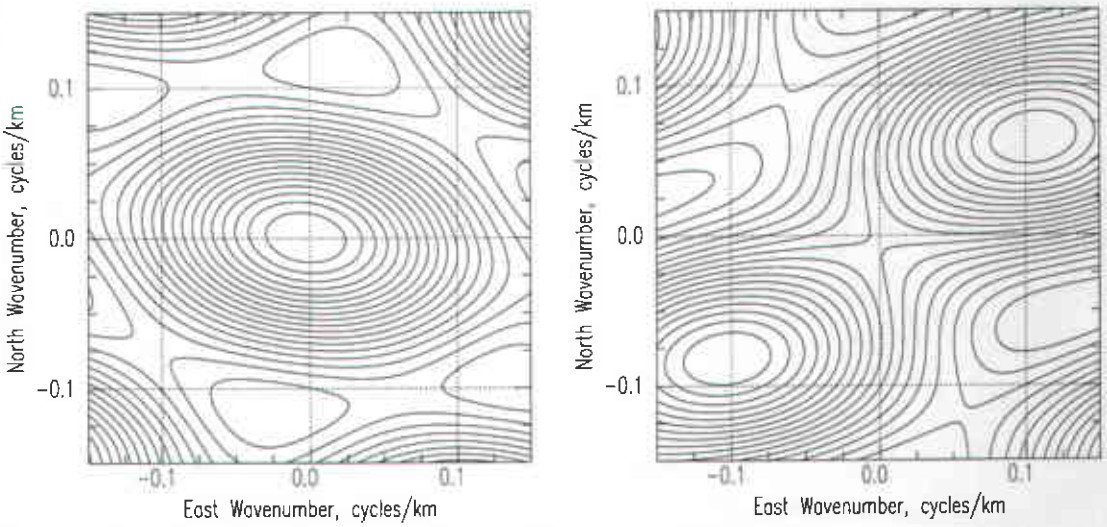

Figure B-3. Examples of wavenumber results for vertical-component ambient noise at Hanford. The frequency band is 100-150 mHz (the peak noise band). The plot on the left shows a result with "infinite" apparent velocity, indicating all three signals are in-phase (as would result of a vertically-propagating body wave). The plot on the right shows a result where there is nearly a 180-degree phase shift at the Southwest End relative to the Corner and Northwest End. Propagation velocity implied is 1 km/s. A 180-degree phase shift corresponds to a wavenumber of 0.125 cycles/km for the peak frequency of 0.125 cycles/s. The wavelength is twice the arm length, and the time-delay is half the period. The propagation direction could be from the northeast or from the southwest.

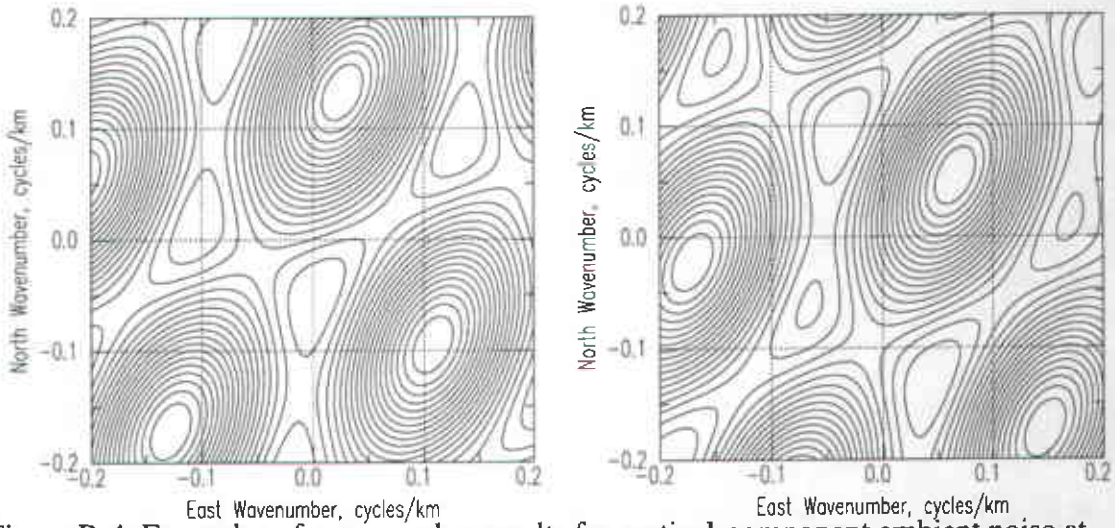

Figure B-4. Examples of wavenumber results for vertical-component ambient noise at Livingston. The frequency band is 150-200 mHz (the peak noise band). The plot on the left shows a result with two peaks on the wavenumber plane that are nearly equidistant from the origin. The wavenumbers corresponding to these peaks are near 0.14 cycles/km, implying a velocity near 1.3 km/s, from north-northeast or southeast directions. Lower velocities are implied by the peaks at west-northwest and southwest azimuths. The plot on the right shows a typical result at Livingston, where the peak on wavenumber plane 0.085 cycles/km from the origin implies a velocity near 2.2 km/s from a northeast azimuth.

Because of the geometry of the array, there are maxima in the wavenumber plane separated every 0.25 cycles/km in directions parallel to the two 4km arms. This cyclic effect, termed beam-pattern, represents potential full-cycle jumps in the cross-correlation of the signals.

Using the f/k >1 restriction eliminates most situations where the peak selected from the wavenumber analysis aligns the noise signals with phase shifts greater than 180 degrees. A more restrictive limit can, however, produce biases because of the "flatter" aperture of the array in the direction parallel to the bisector of the two arms. For example, the phase relationships intermediate to those that produced the wavenumber diagrams in Figure B-4 will preferentially pick a northeastern azimuth of wave approach if a restriction to velocities higher than 1 km/s are considered. A trade-off exists between attempting to fit the data to a model that predicts fast propagation velocities versus a model that suggests southeastern azimuths as possible sources for the noise.

Wavenumber results at Livingston. Figure B-5 shows the result of the wavenumber analysis for the Livingston site in the frequency band 150-200 mHz. At Livingston, the noise is naturally peaked in this frequency range. The three plots on the left of Figure B-5 show the temporal distribution of the 12-hour, moving-window wavenumber analysis. The top plot shows the azimuth estimate, the middle shows the wavenumber estimate, and the bottom shows the peak amplitude of the wavenumber analysis. A slight variation in amplitude over time reflects the overall amplitude variation observed on the spectrograms in Appendix A. The azimuth of wave approach is most frequently from a north or northeast direction (azimuth 0-45 degrees), with azimuths near 135 and 270 degrees occurring less frequently. The middle plot on the left rarely shows wavenumbers less than 0.05 cycles/km, and wavenumbers range from 0.05 to the maximum, 0.20 cycles/s, with no concentrations at any particular value.

The top plot on the right of Figure B-5 shows that most of the low-wavenumber results are associated with azimuths in the 0-45 degree range of approach directions, and the azimuth determinations that cluster near 135 and 270 degrees are associated with the largest wavenumbers (see Figure B-4). It is these latter situations (large wavenumbers) that would indicate slow propagation velocities, large phase differences, and ambiguous phase determinations. The middle plot on the right of Figure B-5 shows that the amplitudes of the wavenumber results outside of the three azimuth groups are systematically smaller than those within the three azimuth groups. The bottom plot on the right shows the amplitude distribution as a function of the wavenumber, and here there is a slight tendency for wavenumbers near 0.10 and from 0.15-0.20 cycles/km to have higher amplitudes.

The most significant result of this analysis is that there are very few instances where the wavenumber of the dominant noise field is less than 0.05 cycles/km. The wavenumber is most frequently near 0.1 cycles/km (and frequently higher), so that the noise propagation velocities are interpreted to be near 2 km/s or slower, given that the dominant frequency is below 0.2 Hz (the peak is near 185 mHz). The low-wavenumber results are primarily associated with a direction of approach of north-northeast. This result is inconsistent with the expected sources in the Atlantic Ocean or other possible sources such as the Gulf of Mexico. The analysis consistently indicates that large phase differences exist, and by

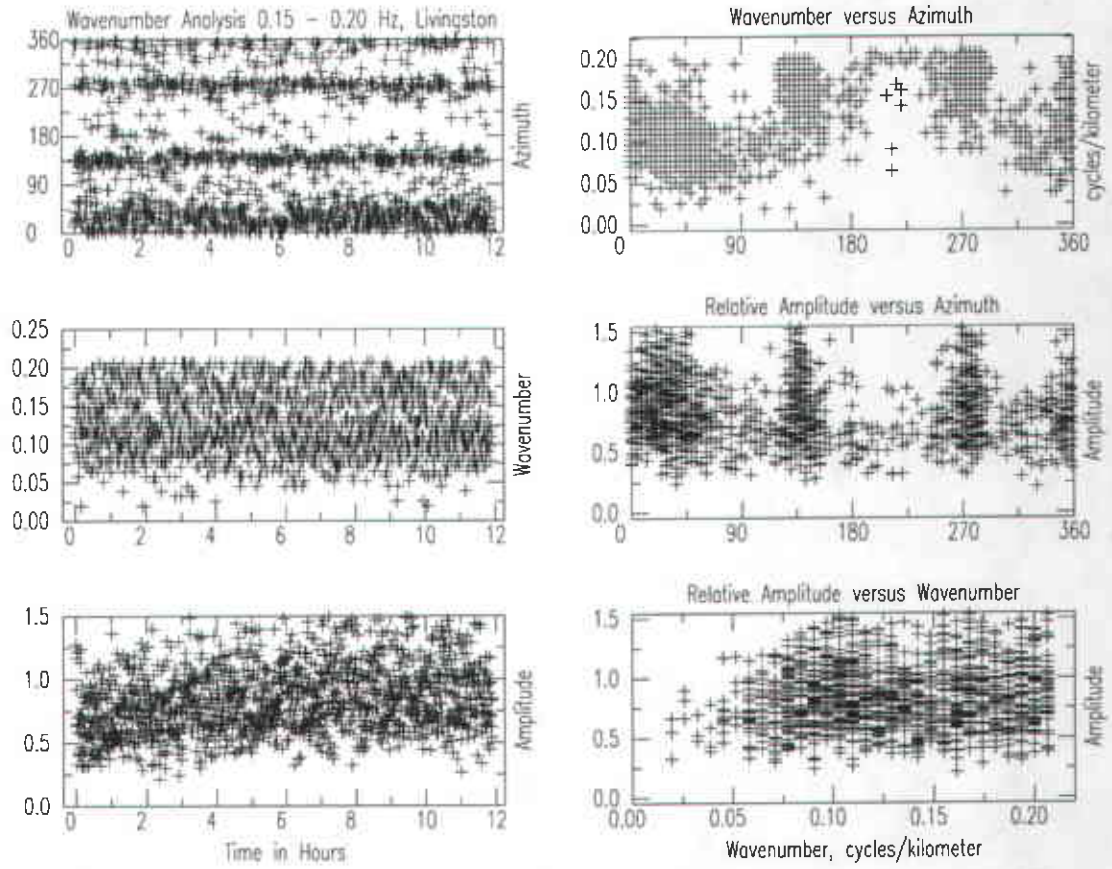

Figure B-5. Wavenumber results for the twelve-hour period at Livingston for the frequency band 150-200 mHz containing the peak noise amplitudes.

restricting the result to minimize the phase differences, the north-northeast direction results. This direction is approximately 45 degrees from the orientation of the two arms, indicating that the Corner is out of phase from either End by about the same amount (1.5 s). For a wavenumber of 0.1 cycles/km, the phase difference is approximately 100 degrees.

Figure B-6 shows the results of a wavenumber analysis for the Livingston data when the time series are filtered to a lower frequency range, 100-150 mHz. This is below the peak frequency analyzed above, so the amplitudes of the wavenumber results are smaller, but similar results are still found. The azimuths are consistently in the north-northeast direction, and the wavenumbers cluster near 0.05-0.07 cycles/km. This again implies propagation velocities near 2 km/s. The concentrations near 135 and 270 degrees are suppressed indicating that these azimuth concentrations are artifacts of the beam-pattern of the tripartite array geometry.

The wavenumber results at Livingston are considerably different from the model of propagating plane waves with velocities above 3 km/s from source regions in oceans or seas. If propagation velocities are instead actually as low as 1 km/s, the wavenumber results could

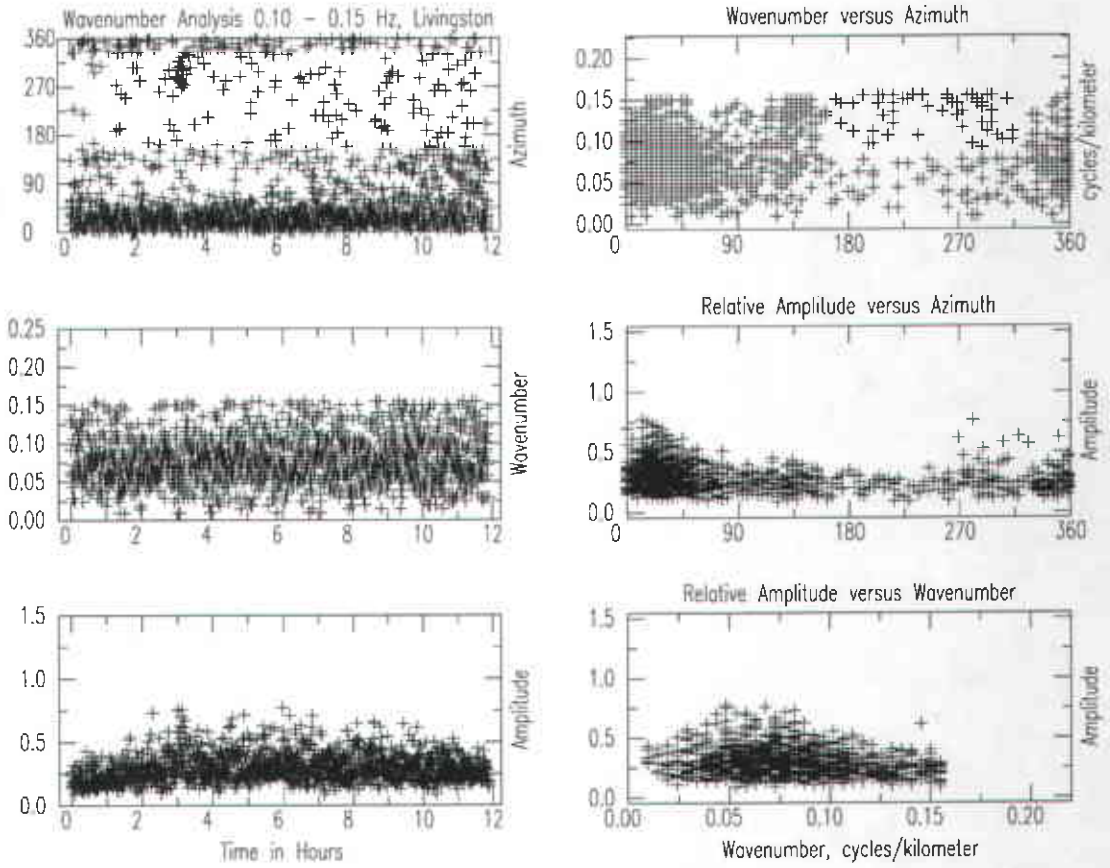

Figure B-6. Wavenumber results for the twelve-hour period at Livingston for the frequency band 100-150 mHz, lower than the peak noise amplitude band.

possibly admit nearly 360 degree phase differences between the two Ends, and intermediate (180 degree) phase differences at the Corner, with propagation from an azimuth of approximately 120 degrees. The azimuth of 120 degrees would appear to be consistent with sources in the Gulf of Mexico, but the propagation velocity required is considered unrealistically low. As noted previously, if the relative phase of the noise is completely random, a concentration of azimuths that bisect the two arms (in the north-northeast or south-southwest) directions could occur when the wavenumber estimate is limited to a small value (maximizing the velocity). The azimuth distribution determined for the Livingston data is consistent with one of these two directions, but the stronger concentration of azimuth estimates from north-northeast directions suggests that the unequal array aperture is not controlling the result.

Wavenumber results at Hanford. Figure B-7 shows the wavenumber results at Hanford for the peak noise frequency 100-150 mHz. The three plots on the left show the temporal distribution of, from top to bottom, the azimuth, wavenumber, and amplitude of the wavenumber analysis. The azimuth of approach of the peak noise is from a wide, generally westerly azimuth range from 180 to 360 degrees, with an additional concentration near a northeastern azimuth of 45 degrees. There appears to be an increasing frequency of the

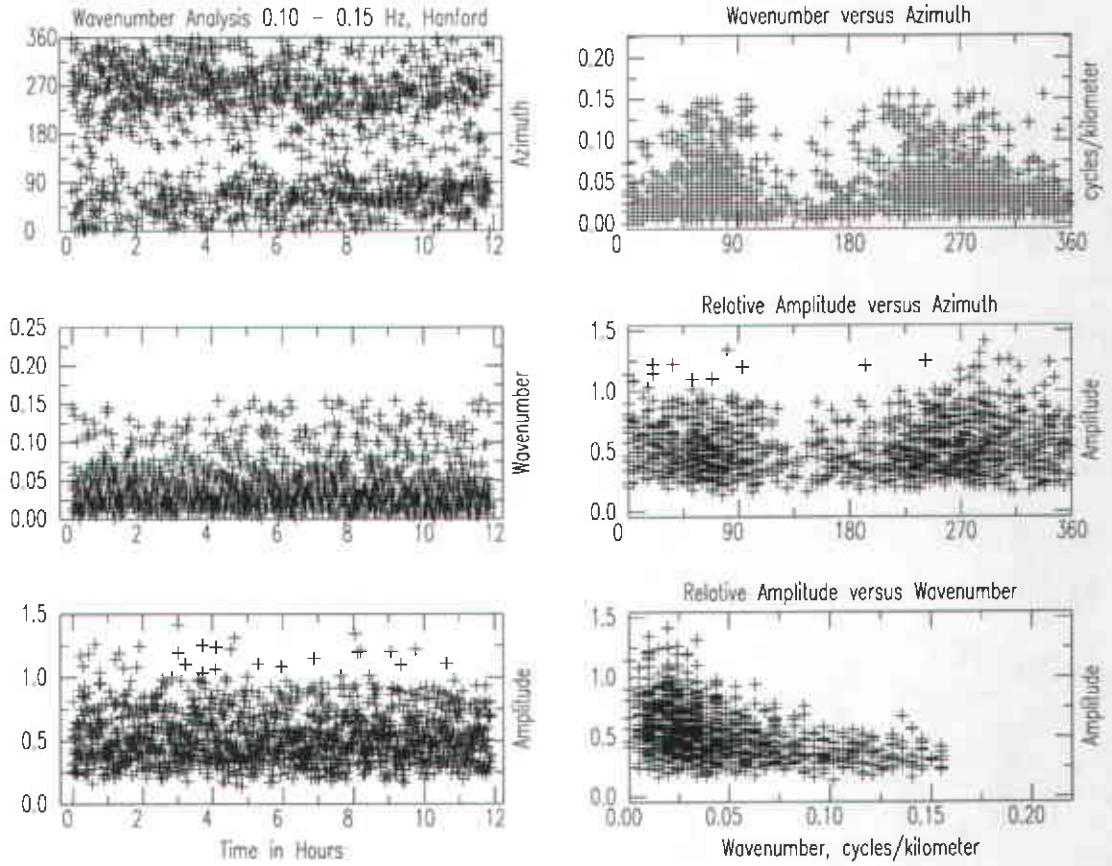

Figure B-7. Wavenumber results for the twelve-hour period at Hanford for the frequency band 100-150 mHz containing the peak noise amplitudes.

northeastern azimuth in the later portion of the time period. The wavenumbers appear to be centered near 0.035 cycles/km. Using the peak frequency of the noise in this range (125 mHz), the velocity determined from the relationship v = f/k is 3.5 km/s.

Figure B-7 also shows, on the right half of the page, that the wavenumber distribution (top) and the amplitude distribution (middle) are similar for either the northeastern or the western azimuths. The bottom plot shows that the higher amplitude wavenumber results (those with high amplitudes and high signal coherence) are concentrated for the wavenumbers below 0.05 cycles/km.

Figure B-8 shows the results of the wavenumber analysis at Hanford in the higher frequency band 150-200 mHz, above the peak frequency at Hanford but at the peak frequency observed at the other site at Livingston. Similar results are found as for the lower frequency band at Hanford, with amplitudes reduced by the fall-off of the underlying noise spectrum.

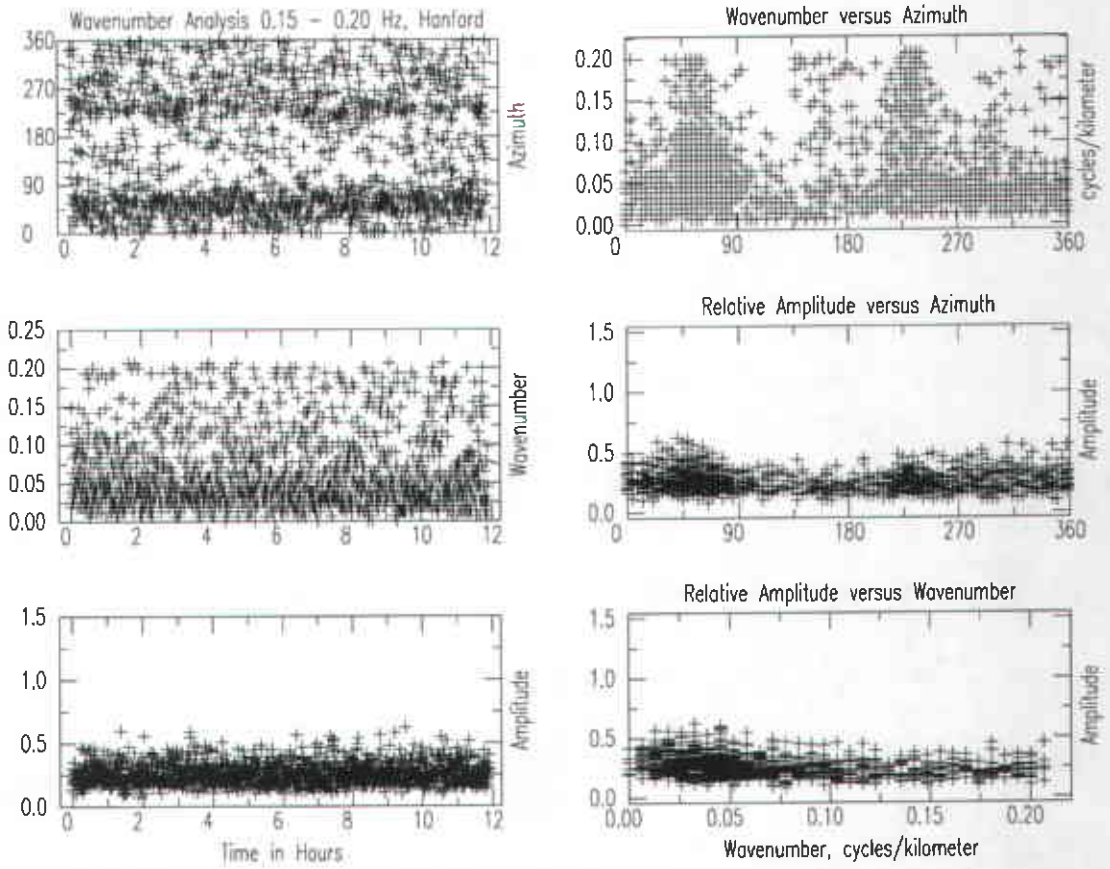

Figure B-8. Wavenumber results for the twelve-hour period at Hanford for the frequency band 150-200 mHz, higher than the peak noise amplitude band.

The wavenumber results at Hanford are generally consistent with the expected model of propagating waves with velocities near 3.5 km/s from sources in the Pacific Ocean. However, there are many periods where much higher velocities are observed (suggesting a body wave component), and there is an additional source of noise that appears to propagate across the site from the northeast.